A critical analysis of plastic flow behaviour in axisymmetric isothermal and Gleeble compression testing

C. J. Bennett[1], S. B. Leen[2], E. J. Williams[1], P. H. Shipway[1], T. H. Hyde[1]

[1]Department of Mechanical, Materials and Manufacturing Engineering

University of Nottingham, Nottingham NG7 2RD, UK

[2]Mechanical and Biomedical Engineering, College of Engineering and Informatics, National University of Ireland, Galway

Abstract

Coupled thermo-mechanical finite element modelling of both isothermal axisymmetric compression and compression testing using the Gleeble thermomechanical simulator has been carried out in order to compare the levels of relative stress error which can arise during each test. A Norton-Hoff material model has been used as a basis for evaluating the testing methods and the calculation of the relative error by providing reference stress-strain curves. The errors arise from effects such as interface friction causing non uniform deformation fields and heat generation in both testing cases and from initial specimen temperature profiles in the case of the Gleeble testing. These errors are shown to be up to approximately 20% and vary throughout the test from positive to negative and are therefore important to consider when processing experimental data.

KEYWORDS: finite element; Gleeble, compression testing; plastic deformation

Nomenclature

Symbol	
A_s	surface area, m^2

B	barrelling coefficient
c	specific heat capacity, J kg^{-1} K^{-1}
D	diameter, m
D_0	initial specimen diameter, m
D_f	final specimen diameter, m
e	emissivity
$e^{\bar{\sigma}}$	stress error
f_s	frictional shear stress, MPa
F	force, N
h	height, m; convection coefficient, W m^{-2} K^{-1}
h_0	initial specimen height, m
h_f	final specimen height, m
$\bar{h}$	average convection coefficient, W m^{-2} K^{-1}
h_0	initial specimen height, m
k	material shear strength, MPa
k	material conductivity, W m^{-1} K^{-1}
K	material consistency, MPa s
L	length, m
L_o	initial specimen length, m
m	coefficient of friction
Nu	Nusselt number
Pr	Prandtl number
r	radius, m
Ra	Rayleigh number
t	time, s
T	temperature, K

T_s	surface temperature, K
T_∞	far field temperature, K
v_0	initial velocity, m s^{-1}
v_h	velocity at height h, m s^{-1}
α	thermal diffusivity, m^2 s^{-1}
β	volumetric thermal expansion coefficient, K^{-1}; material constant, K
ε	strain
ε_p	plastic strain
$\bar{\varepsilon}$	effective strain
$\dot{\varepsilon}$	strain rate, s^{-1}
$\dot{\bar{\varepsilon}}$	effective strain rate, s^{-1}
η	heat generation efficiency factor
μ	coefficient of friction
v	kinematic viscosity, m^2 s^{-1}
ρ	mass density, kg m^{-3}
σ	stress, MPa
$\bar{\sigma}$	effective stress, MPa
$\bar{\sigma}_{ref}$	reference stress, MPa
$\bar{\sigma}_{model}$	calculated model stress, MPa

subscripts

D	diameter
∞	far field condition

1 Introduction

The increased use of finite element codes for the analysis of manufacturing processes often requires material properties over a wide range of temperatures and strain rates. For the modelling of manufacturing processes involving large deformations, an extensive amount of plastic (flow stress) data is required. Typically hot isothermal compression testing is used to generate flow stress data for finite element modelling; this technique is particularly suitable for modelling processes such as rolling and extrusion where the temperature of the workpiece is held approximately constant throughout the process. Compression testing in various guises, (axisymmetric, plain strain and ring tests) has been used to characterize the deformation behaviour of a number of different materials including aluminium [1] and it's alloys [2], steels [3], nickel-based superalloys [4] and nonlinear geomaterials such as rock [5]. However in order to produce material properties for the modelling of manufacturing processes with transient temperature characteristics such as rapid heating rates and steep temperature gradients within the workpiece(s) (friction welding for example), a more suitable testing method is required. Testing using a Gleeble thermo-mechanical simulator is one alternative to isothermal testing as transient temperature conditions can be created to more accurately represent the process being modelled. The Gleeble thermo-mechanical simulator uses electrical resistance heating of the specimen itself which can achieve rapid heating rates to better represent the condition of the material during welding processes; this therefore reduces the effect of changes of the microstructure of materials on their strength (such as the dissolution of γ' in nickel-based superalloys) which can occur during isothermal testing. It is important when material testing is carried out for finite element modelling that the material data accurately represent the condition of the material in the process that is being modelled and that any systematic errors in the testing procedure are understood and accounted for when generating the material dataset.

It has been shown by Evans and Scharning [6, 7] that the presence of unavoidable effects such as interface/contact friction and strain inhomogeneity in the axisymmetric compression testing gives

rise to temperature inhomogeneity in the specimens. This can lead to errors in material properties (stress-strain) derived from such axisymmetric compression tests. They proposed that a finite element model could be used to quantify the level of error in the derived stress-strain characteristics of the material when compared with the actual stress strain response of the material which occurred, and that corrections could be applied to the stress-strain curves generated to give material properties that more accurately represent the material of interest.

Modelling of the temperature distribution in tensile specimens heated by resistance heating in a Gleeble 1500 thermo-mechanical simulator has been carried out by Brown et. al. [8]. Heat transfer coefficients (HTCs) were determined for the contact between the specimen and the water-cooled grips on the Gleeble simulator; these are important in generating the correct temperature profile in the model and understanding this provides a design facility for evaluating grip and specimen geometry, and also for evaluating the effect of thermal parameters on microstructure evolution of the material during the testing.

During Gleeble compression testing, a C-gauge is used to measure the local strain of the specimen at the largest diametric point of the specimen and this is used to calculate the stress. Therefore any errors arising from this measurement method must be understood in order for the flow stress data to be accurate. The finite element models of the compression processes described in this work were produced in order to better understand the compression testing carried out on materials for the modelling of industrial manufacturing processes and the source and magnitude of errors which can occur during the testing.

2 Model Development

Finite element models of both the isothermal compression test and compression testing carried out using a Gleeble thermo-mechanical simulator have been produced using DEFORM-2D, a popular industry tool for simulating rolling [9], extrusion [10], upsetting [11], welding [12] and other forging and forming processes.

The specimen geometry is identical for both types of test, namely cylinders of 12mm in length and 8mm in diameter. In light of the specimen geometry; the modelling can be approximated using an axisymmetric element formulation assuming that there is no misalignment between the specimen and the platens and there are no geometry errors or other initial inhomegeinities which could skew the specimen as these effects cannot be included in the model.

The basic model to represent both compression testing methods is the same and an overview of the model is shown in Figure 1. The specimen is modelled as a rigid-viscoplastic object which assumes that the elastic deformations are negligible and that the total strain is well approximated by the plastic strain ($\varepsilon_T \approx \varepsilon_P$). The platens are modelled as rigid bodies which are meshed to allow for the heat transfer calculations to be performed. Heat transfer with the environment (convection and radiation) is defined on the specimen surface and the contacting surfaces between the specimen and platens have both thermal exchange (conduction) and friction defined.

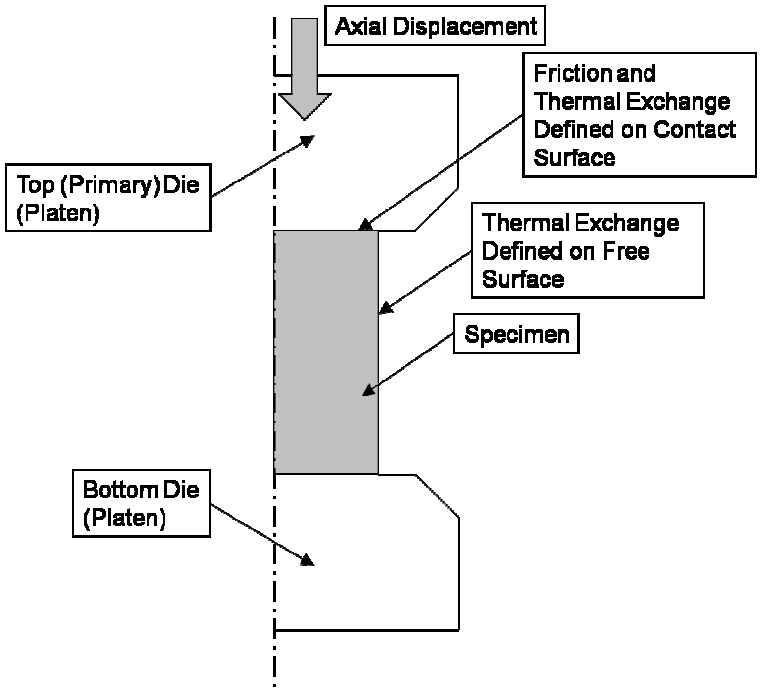

Figure 1: Compression test model

The velocity of the top platen/die is defined as a function of height in the analysis to give a constant macroscopic true strain rate as detailed below:

$$v_h = \frac{-v_0 h}{h_o} \qquad 1$$

The finite element analyses were carried out using time stepping controlled by equal increments of the primary (top) die displacement of 0.1mm. The meshed specimen geometry is shown in Figure 2 with the initial mesh which consists of 507 elements of aspect ratio 1; a typical deformed mesh is also shown at a macroscopic axial true strain of 0.5, the deformation level to which all analyses were run.

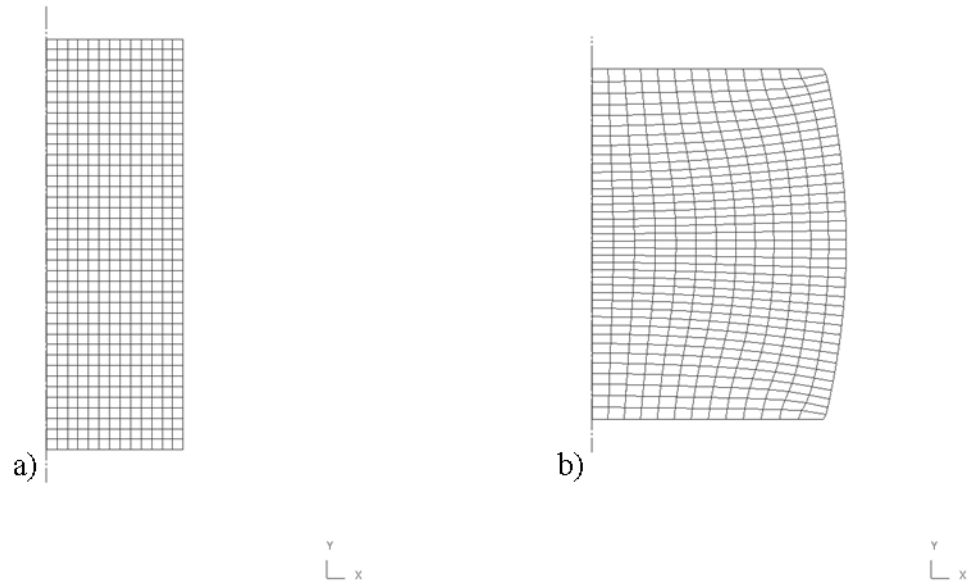

Figure 2: Finite element model of axisymmetric isothermal compression testing

a) Initial mesh; b) Deformed mesh (ε=0.5)

2.1 Material properties

The flow stress of metallic materials typically has a strong dependency on both the temperature and strain rate and also a dependency on strain, $\bar{\sigma} = f(\bar{\varepsilon}, \dot{\bar{\varepsilon}}, T)$. Often this relationship is reasonably described by the classical Norton-Hoff relationship:

$$\bar{\sigma} = K\bar{\varepsilon}^{n}\dot{\bar{\varepsilon}}^{m}\exp\left(\frac{\beta}{T_{abs}}\right) \qquad 2$$

For the purpose of this study, the strain dependency will be assumed to be negligible and therefore the strain exponent n=0, giving:

$$\bar{\sigma} = K\dot{\bar{\varepsilon}}^{m} \exp\left(\frac{\beta}{T_{abs}}\right) \quad (3)$$

As an example, the material of interest for this study is a high temperature nickel-based superalloy, although the techniques described could be applied to any material. The Norton-Hoff law presented in Equation 3 has been fitted using the least squares method to the peak flow stress data obtained from hot axisymmetric compression tests of the nickel-based superalloy and yields the constants presented below:

$K = 4.525\times10^{-4}$ MPa s

$m = 0.167$

$\beta = 18163.2$ K

where K is known as the material consistency, m is the strain rate exponent (sensitivity) and β is a constant related to activation energy. This gives a smooth dataset (with a constant value over the strain range but variation with temperature and strain rate) with which to carry out the comparison between the different material testing techniques. The variation of flow stress with temperature at different constant strain rates is given in Figure 3.

This material model is used throughout this work as the reference or 'ideal' material property and it is therefore useful to define a relative error in stress in order to evaluate the effects in the models as introduced by Evans and Scharning [6]:

$$e^{\bar{\sigma}} = \frac{\bar{\sigma}_{model} - \bar{\sigma}_{ref}}{\bar{\sigma}_{ref}} \quad (4)$$

Thermal properties of the material are also required to perform the thermo-mechanical finite element modelling of the compression tests. Thermal conductivity and heat capacity are approximated by linear relationships with temperature (fitted using data for the temperature range 800-1150°C [13], Equations 5 and 6 respectively):

$$k = 0.05T - 14.7 \quad (5)$$

$$c_p = 0.0093T - 1.9431 \quad (6)$$

Emissivity is also considered taking a value of 0.7, typical of polished nickel [14].

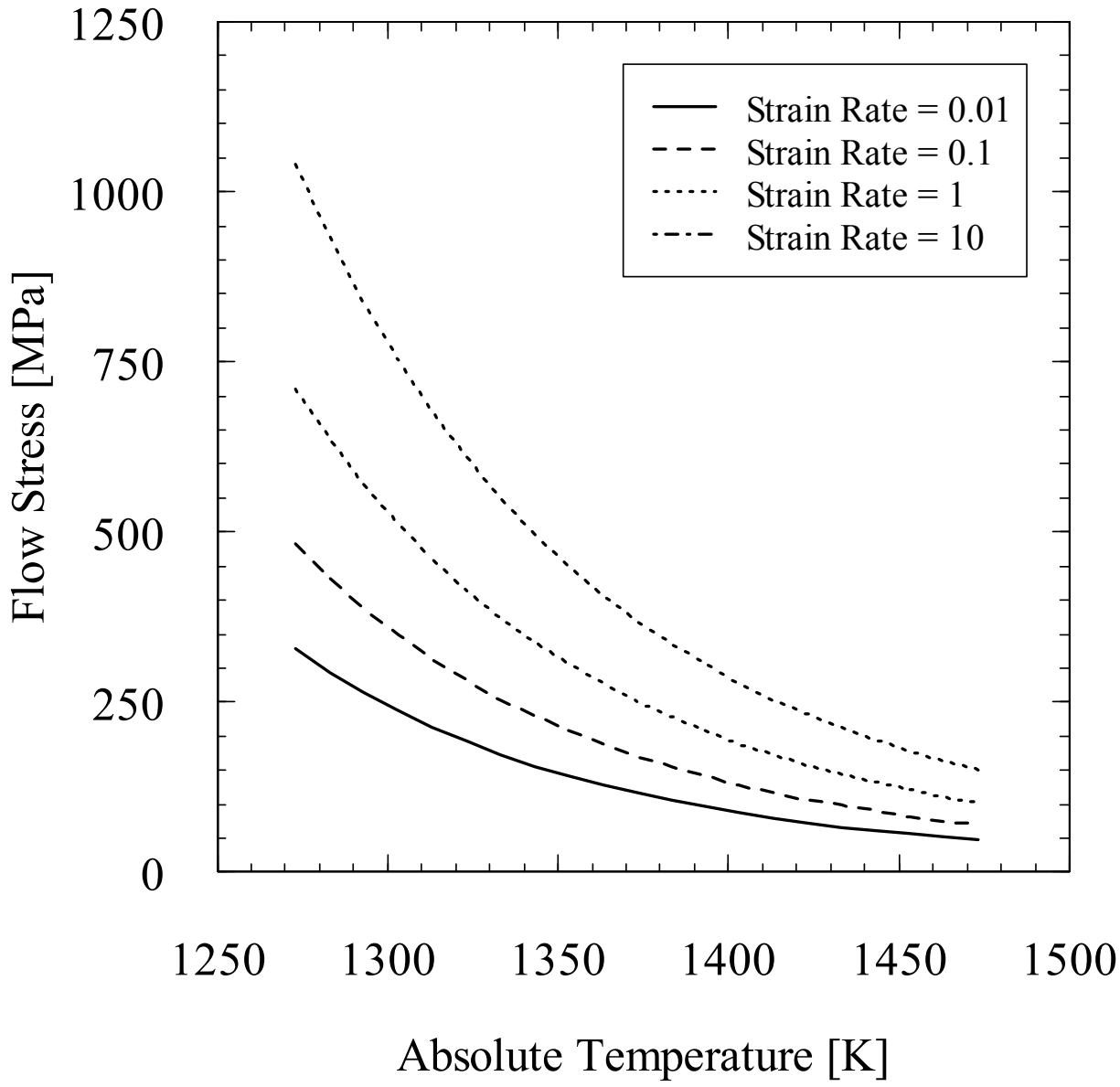

Figure 3: Flow stress variation with temperature and strain rate for the nickel-based superalloy as defined by Equation 3

2.2 Interface friction

In experimental material compression testing, the coefficient of friction between platens and specimen is reduced by the use of lubricant films. It is important to understand how friction affects the stress-strain outputs from the material testing.

The frictional shear stress, f_s is commonly represented using one of the two following relationships:

$$f_s = \mu p \tag{7}$$

where p is a compressive normal stress and μ is the coefficient of friction, or:

$$f_s = mk \tag{8}$$

where m is the friction coefficient ($0 \leq m \leq 1$) and k is the shear strength of the material. Equation 8 is commonly used in the analysis of bulk metal forming while Equation 7 is more suited to the representation of the friction shear stress during sheet metal forming. This arises due to the compressive normal stress at the surface in sheet metal forming being relatively low compared to that observed in bulk metal forming. Typical values for m are given as [15]:

m = 0.2-0.4 for hot forging of steel and copper alloys at high temperatures with graphite based lubricants

m = 0.1-0.3 for hot forming of titanium or other high temperature alloys with glass lubricants.

Friction at the interface between the specimen and the platens is a source of strain inhomogeneity in the compression specimen and results in non-uniform deformation of the specimen as shown in Figure 2b. This non-uniformity is known as *barrelling* [16].

3 Isothermal Compression Test Model

In order to simulate the isothermal conditions imposed in the compression testing, the initial conditions for this model are that the specimen, platens and environment are all initially at the test temperature T_{test}.

3.1 Interface friction without heating due to plastic deformation

Analyses have been carried out investigating the variation in load with changing friction coefficient on the isothermal model at 1100°C tested at a strain rate of $1s^{-1}$; the predicted deformed shape is shown in Figure 4 and the load-displacement results are shown in Figure 5. A slight variation is shown in the load displacement curves as the friction coefficient is increased since initial loads have to be higher to overcome the friction at the interface.

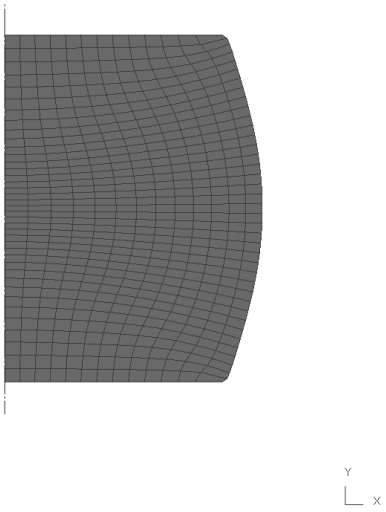

Figure 4: Typical deformed mesh of isothermal compression test model (T=1100°C, $\dot{\varepsilon}$=$1s^{-1}$, ε=0.5, m=0.3, no re-meshing)

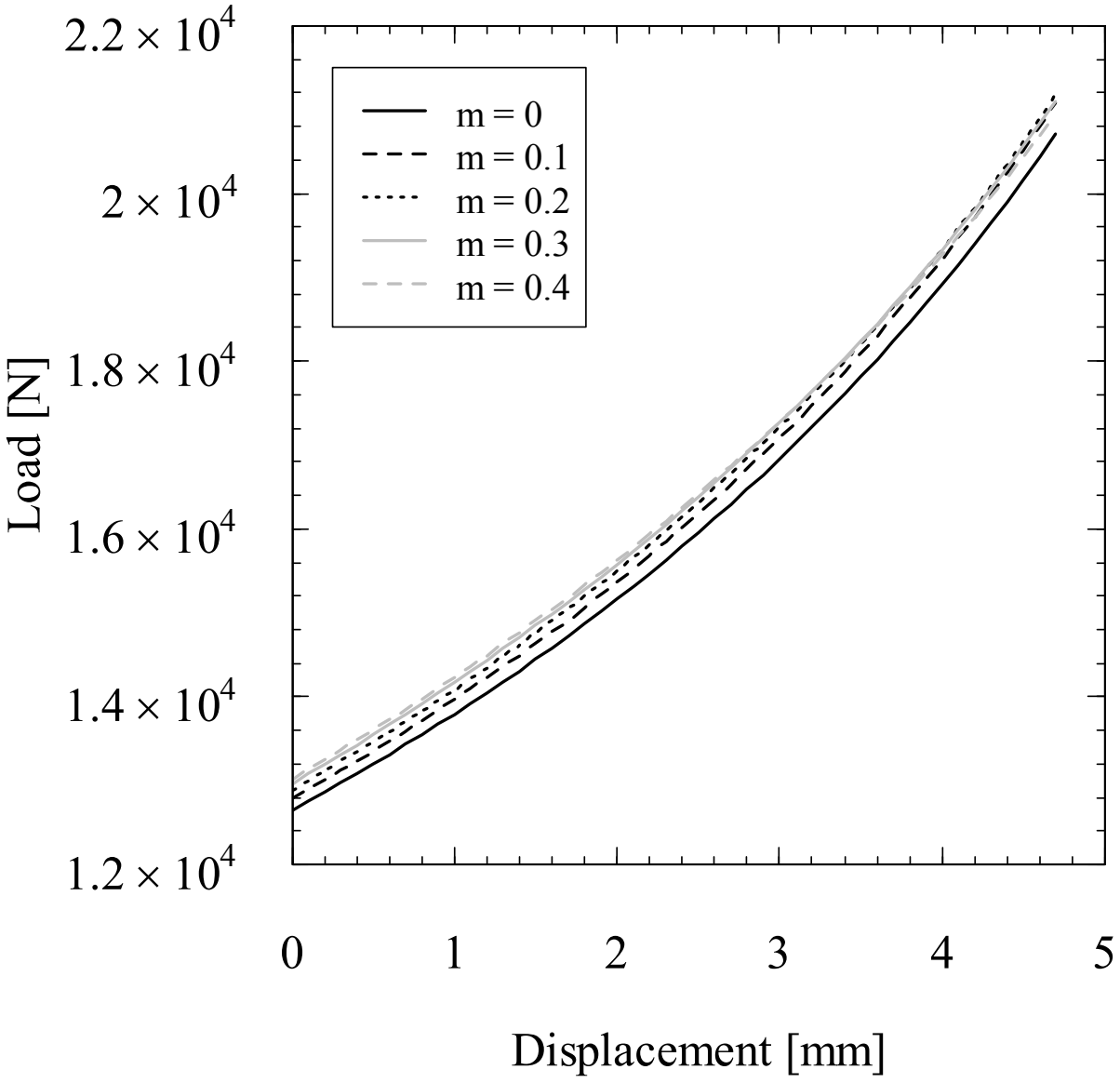

Figure 5: Effect of *m* on load-displacement results from isothermal model (*T*=1100°C, $\dot{\varepsilon}$=1s^{-1})

The load-displacement data presented in Figure 5 can be converted to stress-strain data for comparison with the Norton-Hoff material model which will allow for stress errors to be calculated. True strain can be calculated from the axial displacement data using:

$$\varepsilon = \ln\left(\frac{L_0 + \Delta L}{L_0}\right) \qquad 9$$

Stress is calculated assuming constant volume of the testpiece and that the cylindrical shape is maintained throughout the test. As such:

$$\sigma = \frac{F}{\frac{\pi D_0^{\,2}}{4}\frac{L_0}{L_0 + \Delta L}} \qquad 10$$

Stress-strain curves derived from the load-displacement data extracted from the models presented in Figure 5 are shown in Figure 6. It can be seen that the peak stress is predicted to increase with increasing friction between the specimen and platens.

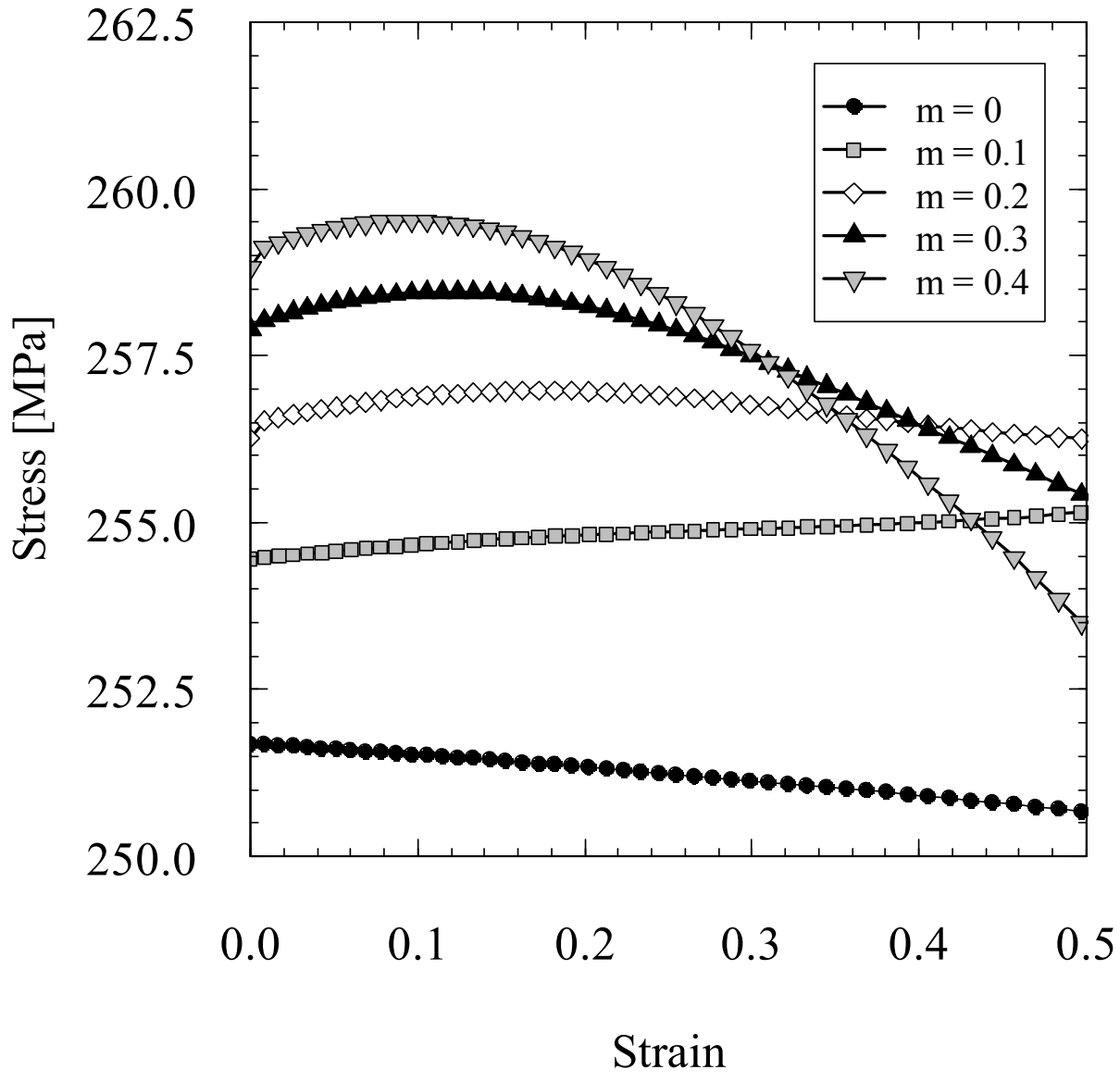

Figure 6: Effect of *m* on stress-strain curves from isothermal model (*T*=1100°C, $\dot{\varepsilon}$ =1s^{-1})

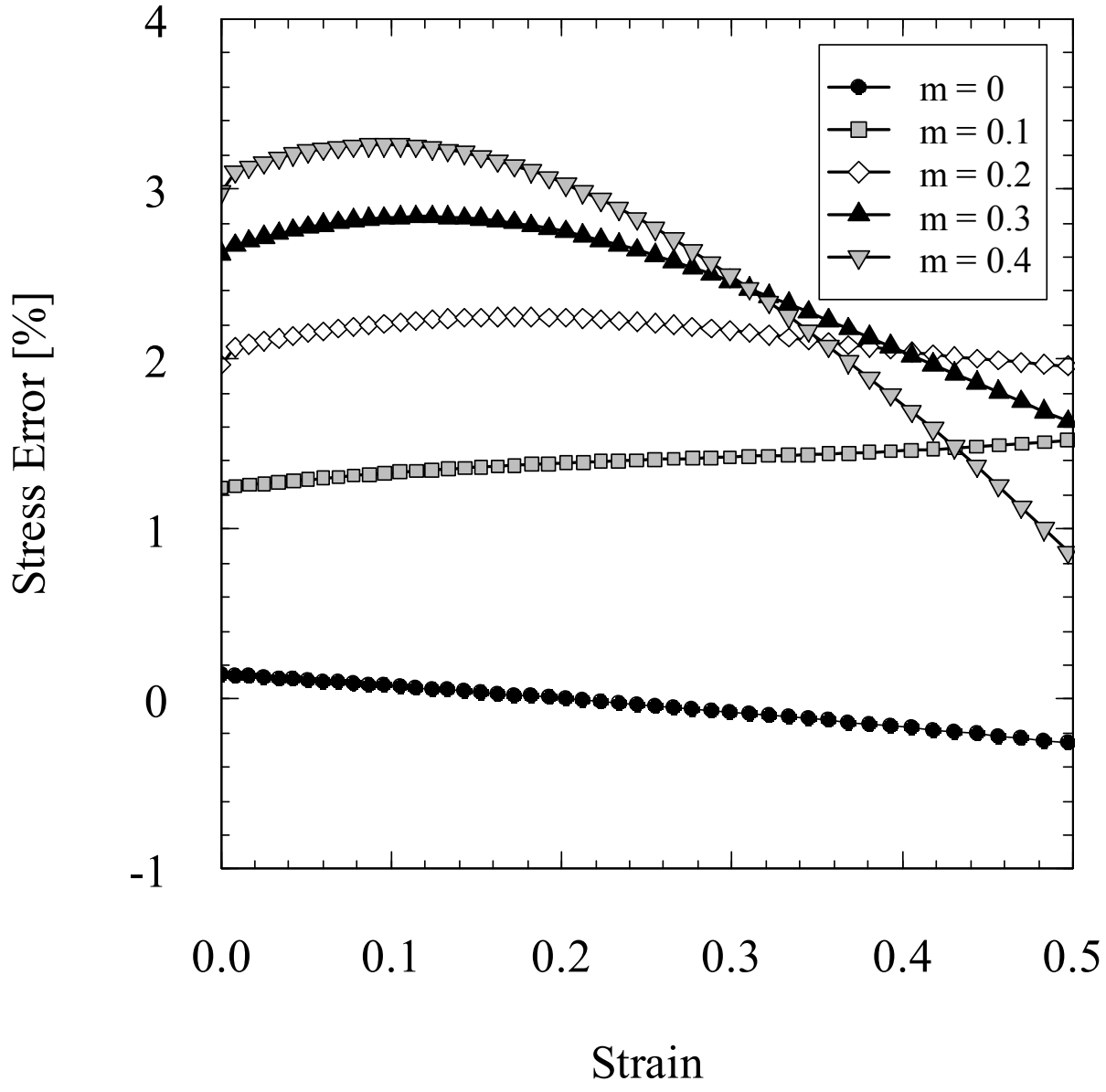

Figure 7: Relative error in stress from isothermal model for varying *m* (*T*=1100°C, $\dot{\varepsilon}$=1s^{-1})

The relative error in stress (as defined in Equation 4) when compared to the value from the material model (Equation 3) is presented in Figure 7. It can be seen that, for zero friction, the error is very small, as expected. The peak error increases with increasing friction coefficient, *m* up to approximately 3.25% for an *m* value of 0.4, as more load is required to deform the specimen (overcome the interface friction). The effect of interface friction on specimen deformation is shown in Figure 8; here, it can be seen that without interface friction (*m* = 0.0) the strain rate axially along

the centre of the specimen is constant whereas for higher levels of friction (m = 0.4 in this case) mechanical constraint is applied to the end of the specimen and deformation rates are higher at the specimen centre which produces the barrelled geometry also shown in Figure 8.

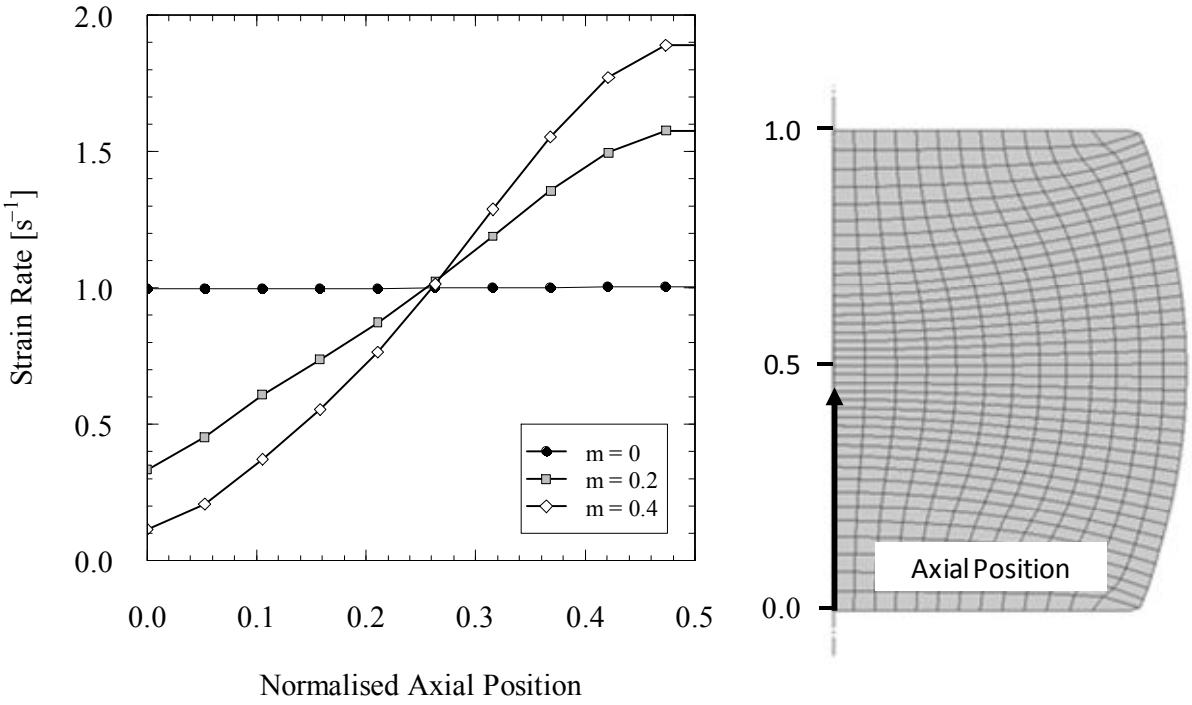

Figure 8: Strain rate along the centreline of the isothermal model at a macroscopic true strain of 0.5 (T=1100°C, $\dot{\varepsilon}$=1s^{-1}, ε=0.5)

The barrelling coefficient, B, is a measure of the level of inhomogeneity in the deformation of the specimen induced by the interface friction and is defined as [16]:

$$B = \frac{h_f {D_f}^2}{h_0 {D_0}^2} \qquad 11$$

Excessive barrelling can result in increased uncertainties in the flow stress values produced during a test; tests with values of barrelling coefficients greater that 1.10 are considered invalid.

Theoretically *B* has a value of 1 when there is no barrelling present. The values of *B* have been calculated for the analyses shown in Figure 5 and are presented in Figure 9 as a function of *m*. It is shown that the barrelling coefficient has a value of approximately 1.0 when there is no friction present. It is also noted that *B* is more sensitive at low values of *m*.

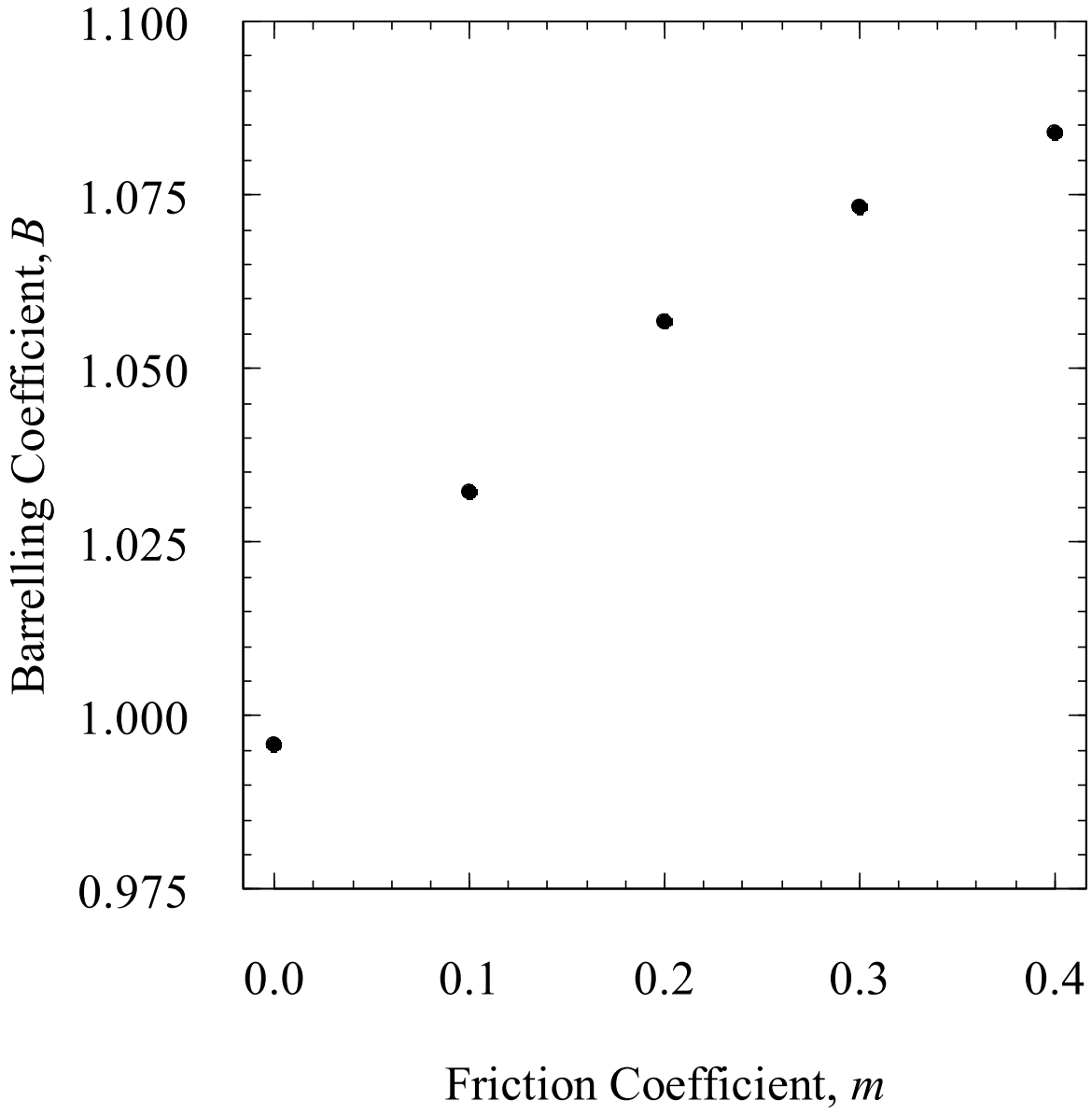

Figure 9: Variation in Barrelling Coefficient, *B* in isothermal models with *m* (*T*=1100°C, $\dot{\varepsilon}$ =1s^{-1}, ε=0.5)

3.2 Heat generation due to plastic deformation without friction effects

Both plastic deformation and frictional work contribute to heat generation in metal forming. The temperature rise in the specimen that occurs due to the conversion of mechanical energy to heat energy can be responsible for softening during material testing as the strength of a material is temperature dependant, an increase in temperature normally corresponding to a lower strength. The heat generation efficiency factor, η determines the ratio of mechanical energy converted to heat in the finite element modelling and has typical values in the range 0.9-0.95. The remainder of the energy is expended as changes to dislocation density, grain boundaries and phase makeup [15]. In order to assess the significance of the effect of η on the temperature profile of the specimen, models were run at T=1100°C, $\dot{\varepsilon}$=1s^{-1}, $\dot{\varepsilon}$=10s^{-1}, with mechanical to heat conversion factors of η=0.9 and η=0.95 (m=0). The heat generation rate is given by [15]:

$$\dot{r} = \eta \sigma_{ij} \dot{\varepsilon}_{ij} \qquad 12$$

So it can be seen that the heat generation rate is a function of the stress and strain rate and therefore will be more important at lower temperatures and higher strain rates due to the increased strength of the material.

Table 1: Maximum temperature rise, dT in °C at ε=0.5

η	1100°C, 1s^{-1}	1100°C, 10s^{-1}
0.9	13.7	19.5
0.95	14.4	20.5

The maximum temperature rise is shown in Table 1 at a macroscopic axial true strain of 0.5. It can be seen that although there is a clear difference between the two values with η=0.9 and 0.95, the difference between the two values is less than 0.1% of the initial temperature of the specimen in this case. Therefore, for further work a value of η=0.9 was used.

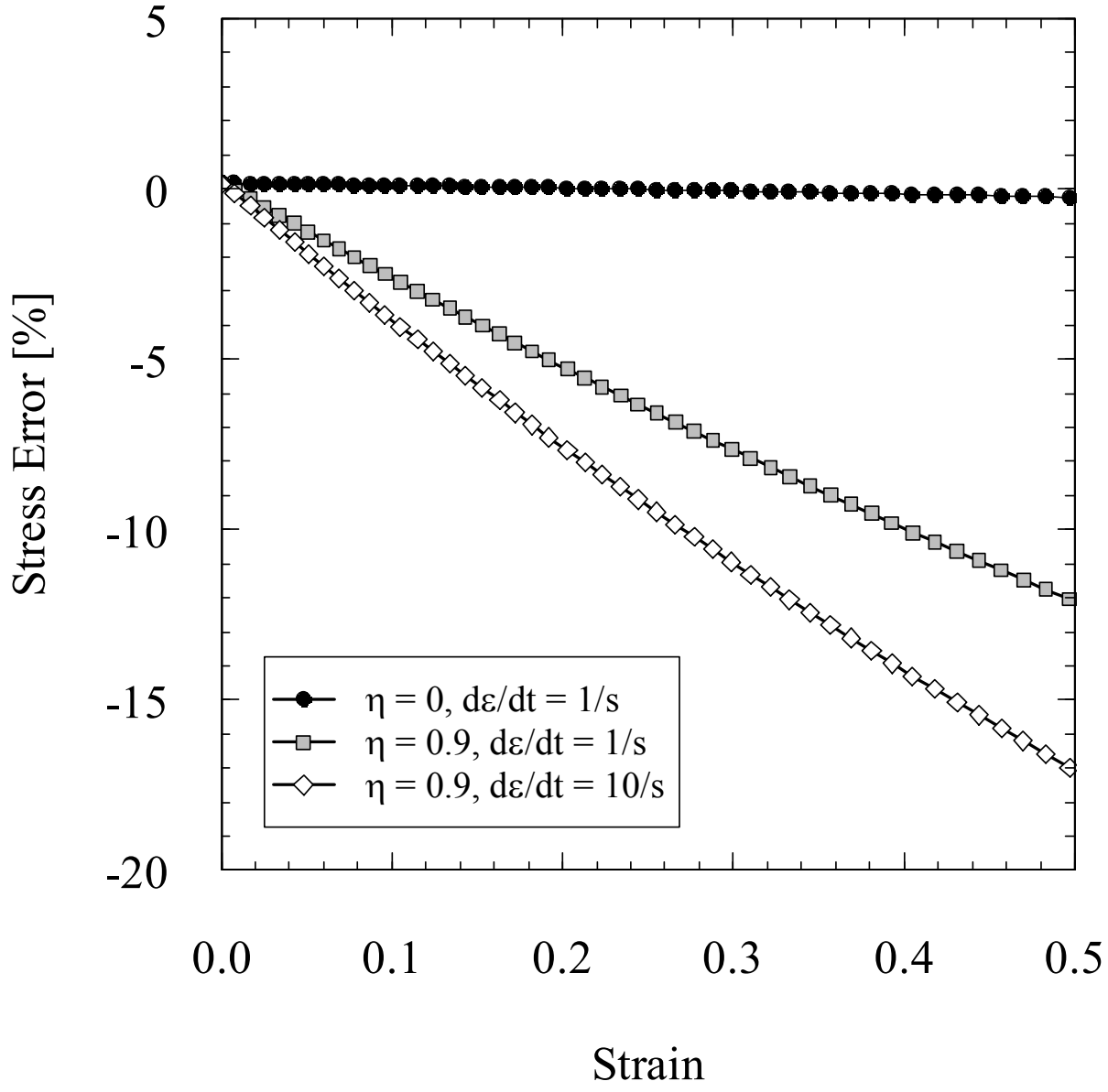

Figure 10: Comparison of stress errors from isothermal models with η=0.0 and η=0.9 (m=0 in all cases)

A comparison of the relative stress errors generated when including the mechanical energy to heat conversion with the situation where η=0 is shown in Figure 10. In both cases m=0 and so the error arises entirely from the conversion of mechanical energy to heat; a decrease of approximately 12% can be seen at the final strain value in the model at a strain rate of $1s^{-1}$ with η=0.9. The relative

stress error increases to around 17% when the strain rate is increased to $10s^{-1}$ due to the additional heating that this causes. Temperature rises of 14°C and 19.5°C in the material model gives flow stress drops of approximately 12.5% and 17% respectively compared to the value at 1100°C so the errors presented in Figure 10 agree very well with the values of stress drop expected from the temperature rise. This highlights the importance of including this phenomena in the modelling of compression testing and indicates that it could be responsible for considerable flow softening in material testing.

3.3 Combined effects of friction and heat generation due to plastic deformation

When the effects of both interface friction and heat generation due to plastic deformation are added to the model, the relative stress errors from various interface friction coefficients are as shown in Figure 11. This shows initial positive errors due to the presence of the interface friction which reduce with increasing strain due to the effects of heating from plastic deformation. In all cases, at a macroscopic axial true strain of 0.5 the errors are negative and in the order of 10-12% for this test condition (T=1100°C, $\dot{\varepsilon}=1s^{-1}$, η=0.9). These are significant error values and it is necessary that these are considered when analysing results generated in isothermal compression testing.

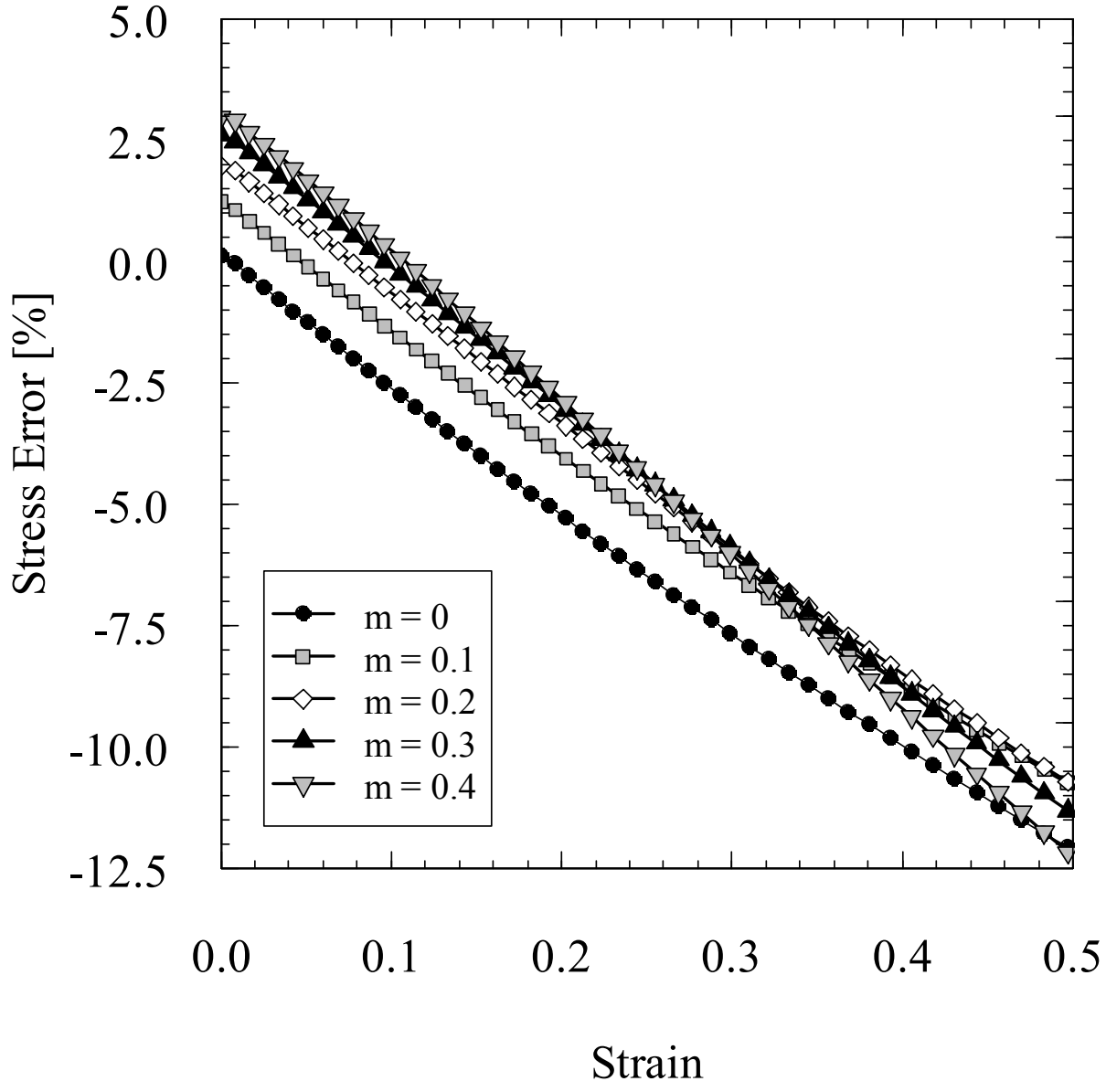

Figure 11: Relative error in stress from isothermal models with combined friction effects and heating from plastic deformation (T=1100°C, $\dot{\varepsilon}$=1s^{-1}, η=0.9).

4 Gleeble Compression Test Model

The test specimens for the compression testing carried out using a Gleeble thermo-mechanical simulator have the same geometry as those typically used for isothermal axisymmetric compression

testing (8mm diameter by 12mm long cylinders). The specimens are heated using resistance heating following Joule's Law:

$$Q \propto I^2 R \qquad 13$$

A current is passed through the specimen and the power dissipated at any point is proportional to the electrical resistance of the conductor. The power dissipated varies with temperature as the resistivity of a material is temperature dependent. This phenomenon can be modelled using DEFORM-2D.

The experimental strain is measured using a C-gauge at the axial centre of specimen (largest diameter point), which is then used to calculate stresses and strains. The coupled effects of resistance heating and cooled grips causes a temperature profile in the specimen and it is important to understand the effect this has on the stress-strain curves generated and how these compare to true isothermal behaviour.

4.1 Heat loss from the specimen during heating

In order to model the resistance heating used in the Gleeble using DEFORM-2D, additional material properties are required. These include temperature dependent emissivity values; values for pure nickel were available from the literature (Figure 12) [14] and are considered to be appropriate for these analyses. Resistivity values are also required to model the resistance heating and data for the nickel-based superalloy Nimonic 80A have been presented by Wilthan et. al. [17] (Figure 13) and are used for the analyses in this paper.

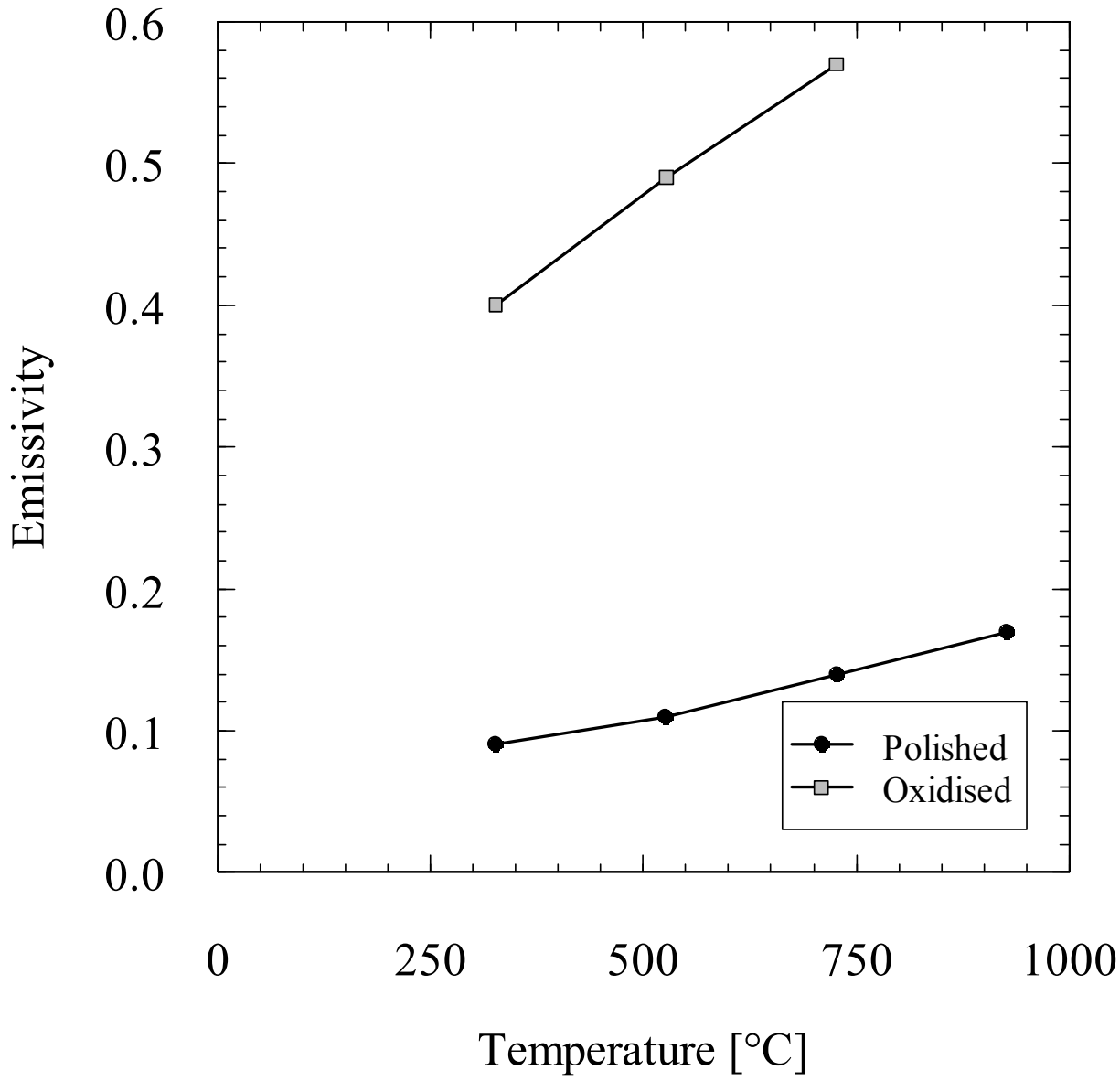

Figure 12: Temperature dependent emissivity values for pure nickel [14]

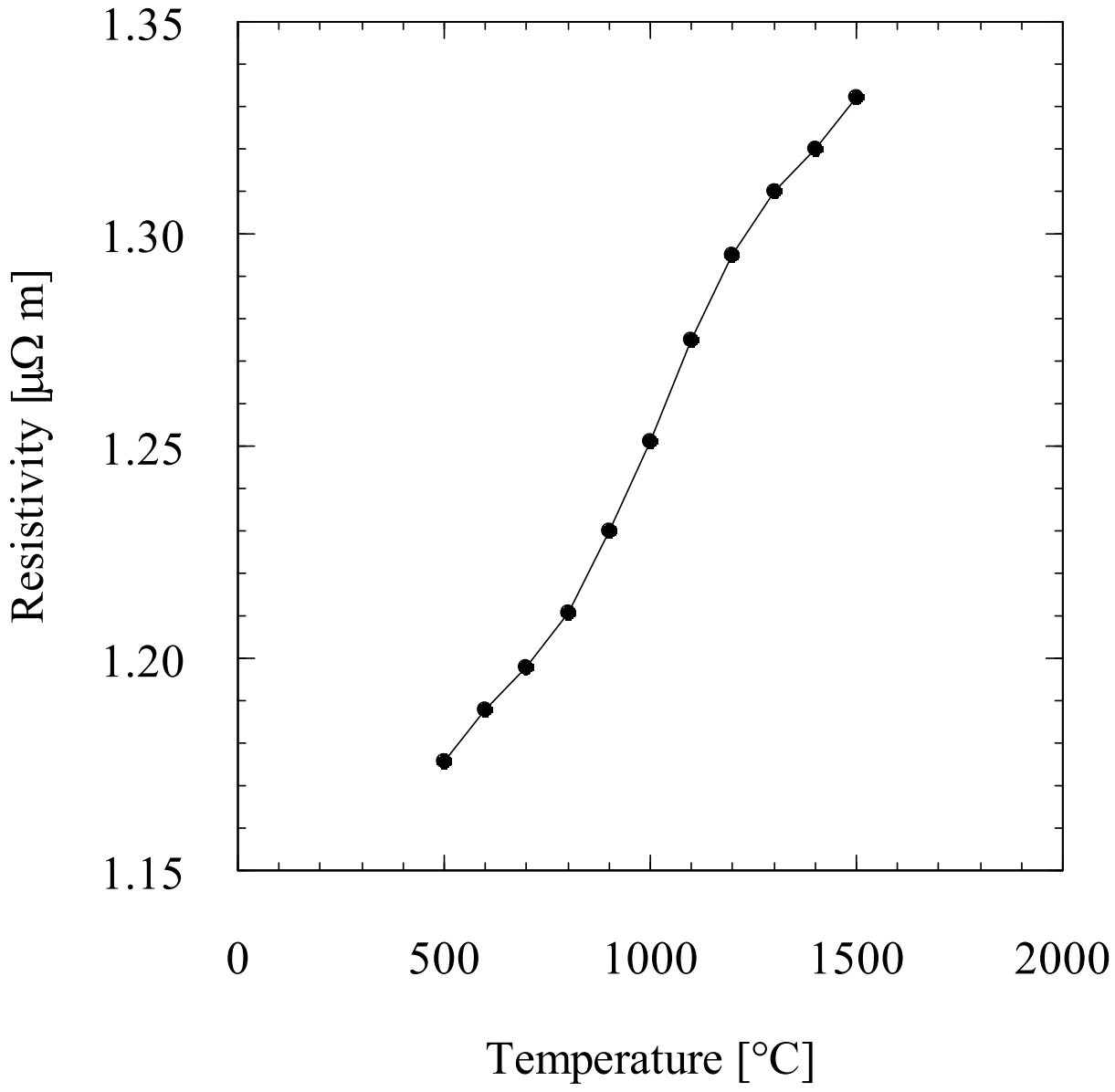

Figure 13: Temperature dependent resistivity values for Nimonic 80A (reproduced from [17])

Surface heat transfer coefficients (HTCs) have been analysed using convective heat transfer theory in relation to free convection around a horizontal cylinder. It is assumed that the surface of the specimen is small in relation to the surroundings and that the air is quiescent.

The surface temperature of the specimen is known as the Gleeble control system uses a thermocouple welded mid way along the axial length of the specimen. These data can be used to

determine the surface HTC by assessing the Nusselt number which is a dimensionless parameter which provides a measure of the convection heat transfer occurring at the surface. The single correlation for the average Nusselt number over a wide Rayleigh number range was recommended by Churchill and Chu [18]:

$$\overline{Nu}_D = \left\{ 0.60 + \frac{0.387 Ra_D^{1/6}}{\left[1 + (0.559/\mathrm{Pr})^{9/16}\right]^{8/27}} \right\}^2 \quad \text{for } Ra_D \leq 10^{12} \qquad 14$$

Applying this to the Gleeble specimen geometry and temperatures and using properties of air at atmospheric pressure and assuming an average temperature between the T_s and T_∞:

$$Ra_D = \frac{g\beta(T_s - T_\infty)D^3}{\nu\alpha} \qquad 15$$

where:

$$\beta \approx -\frac{1}{\rho}\frac{\rho_\infty - \rho}{T_\infty - T} \qquad 16$$

ρ = 0.2488kgm^{-3} [14] ρ_∞ = 1.1614kgm^{-3} [14], T_∞ = 300K and T = 1400K, g = 9.81ms^{-2}, D = 8.0×10^{-3}m, ν = 93.8×10^{-6}m^{2}s^{-1} [14] and α = 131×10^{-6}m^{2}s^{-1} [14] which gives Ra_D = 1.50×10^3. Combining this with the Prandtl number, Pr = 0.716 [14] in Equation 14, this can then be used to evaluate the Nusselt number for this situation and gives $\overline{Nu}_D$ = 2.85.

The average heat transfer coefficient can be calculated using:

$$\bar{h} = \frac{k}{D}\overline{Nu}_D \quad (17)$$

which gives $\bar{h}$ = 21.2W/m^2 K.

Another method of assessing the Nusselt number was presented by Morgan [19]:

$$\overline{Nu}_D = \frac{\bar{h}D}{k} = CRa_D{}^n \quad (18)$$

The constants C and n were given for various ranges of Ra_D values for which C = 0.85 and n = 0.188 for the range $Ra_D = 10^2$-10^4, this gives the Nusselt number $\overline{Nu}_D$ = 3.42 which in turn gives $\bar{h}$ = 25.5W/m^2 K.

Assuming a steady-state local condition considering resistance heating and that $Q_{in} = Q_{out}$ given by:

$$\dot{q} = \frac{2h(T_s - T_\infty)}{r_0} \quad (19)$$

the theoretical radial temperature profile can be shown to be given by:

$$T(r) = T_s + \left(\frac{\dot{q}r_s{}^2}{4k}\right)\left(1 - \frac{r^2}{r_s^2}\right) \quad (20)$$

The calculated radial temperature profiles using Equation 20 are shown in Figure 14 for the previously calculated values of $\bar{h}$. It is shown that the radial temperature variation in the specimen

is less than 2°C at 1100°C for all values of $\bar{h}$. Therefore a value of 20.0Wm^{-2} was used as the surface heat transfer coefficient for the Gleeble modelling carried out here.

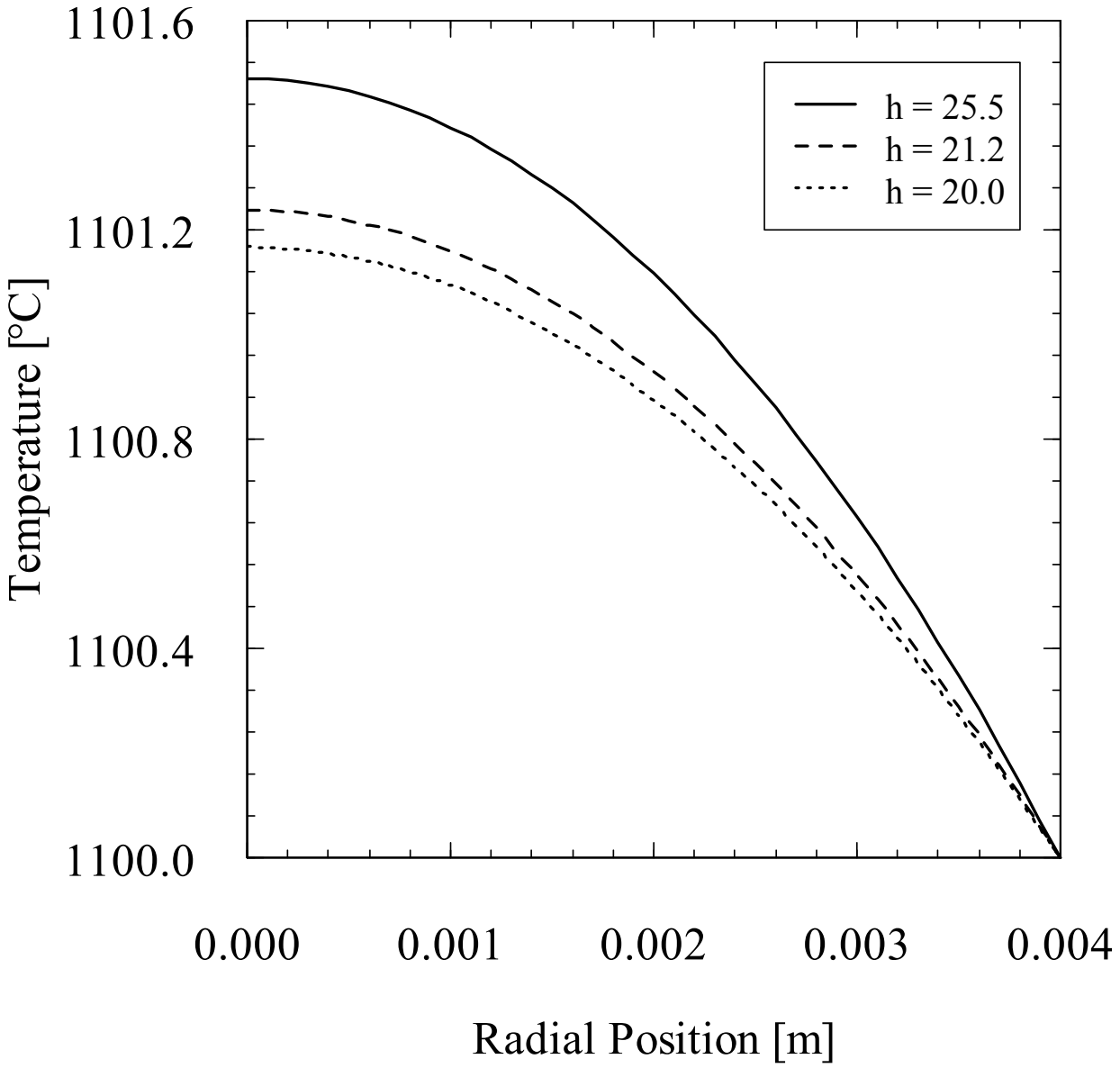

Figure 14 Theoretically-calculated radial temperature distribution in the Gleeble specimen at 1100°C assuming steady-state conditions for different values of $\bar{h}$

4.2 Axial temperature profile

Experimental cooling data, available for the temperature range 800-200°C [20], can be used to evaluate the contact heat transfer coefficients and assuming that the temperature profile in the specimen is uniform and that the decrease in temperature is dominated by the heat transfer, the system can be assumed to be a lumped capacitance type system, obeying the following relationship [14]:

$$-hA_s(T - T_\infty) = \rho Vc \frac{dT}{dt} \qquad 21$$

as the temperature-time history is known from experimental measurements. The contact heat transfer coefficient, h, which represents the heat transfer characteristics of the contact and the lubricant film between the specimen and the cooled platens can be determined as a function of specimen temperature by rearranging Equation 21:

$$\frac{T - T_\infty}{T_i - T_\infty} = \exp\left[-\left(\frac{hA_s}{\rho Vc} \right) t \right] \qquad 22$$

giving the following expression for h:

$$h = -\left[\frac{\ln\left(\frac{T - T_\infty}{T_i - T_\infty} \right) \rho Vc}{A_s t} \right] \qquad 23$$

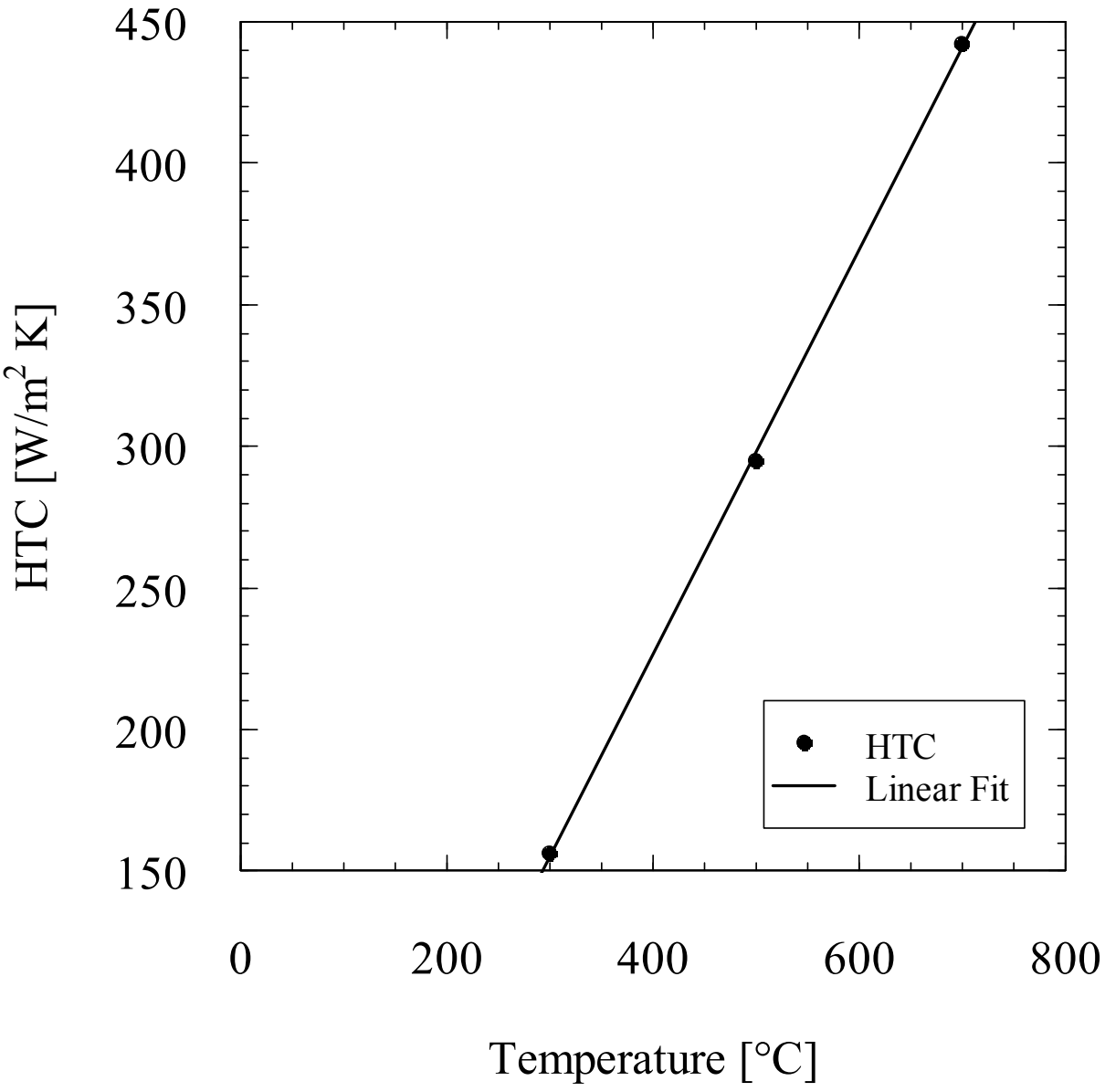

Figure 15: Calculated contact HTCs from Gleeble cooling data as a function of temperature

The HTC was evaluated using three temperature ranges using Equation 23 (800-600°C, 600-400°C and 400-200°C) over the entire cooling data to give a relationship of HTC with temperature, material properties at the mid-range temperature value (700, 500 and 300°C respectively) were used in the calculations. The relationship of the heat transfer coefficient to temperature is shown in Figure 15; it can be seen that the relationship is linear and this relationship was coded into a user subroutine to define the contact HTC. It was assumed that equal heat transfer occurred on both

contacting surfaces and that the HTC value was independent of radial contact position. A constant value of contact HTC was also calculated using the whole cooling range (800-200°C) and the material properties at 500°C. A comparison of the experimental and DEFORM Gleeble cooling model results are shown in Figure 16. The results of two models are presented, the first using the constant HTC determined using the whole cooling range (800-200°C) ("Model – Constant HTC") and the second using the HTC subroutine ("Model – Subroutine HTC") containing the linear relationship of HTC with temperature shown in Figure 15. It can clearly be seen that varying the contact HTC with temperature has a significant effect on the prediction of the cooling profile from the model and improves the agreement with the experimental data considerably.

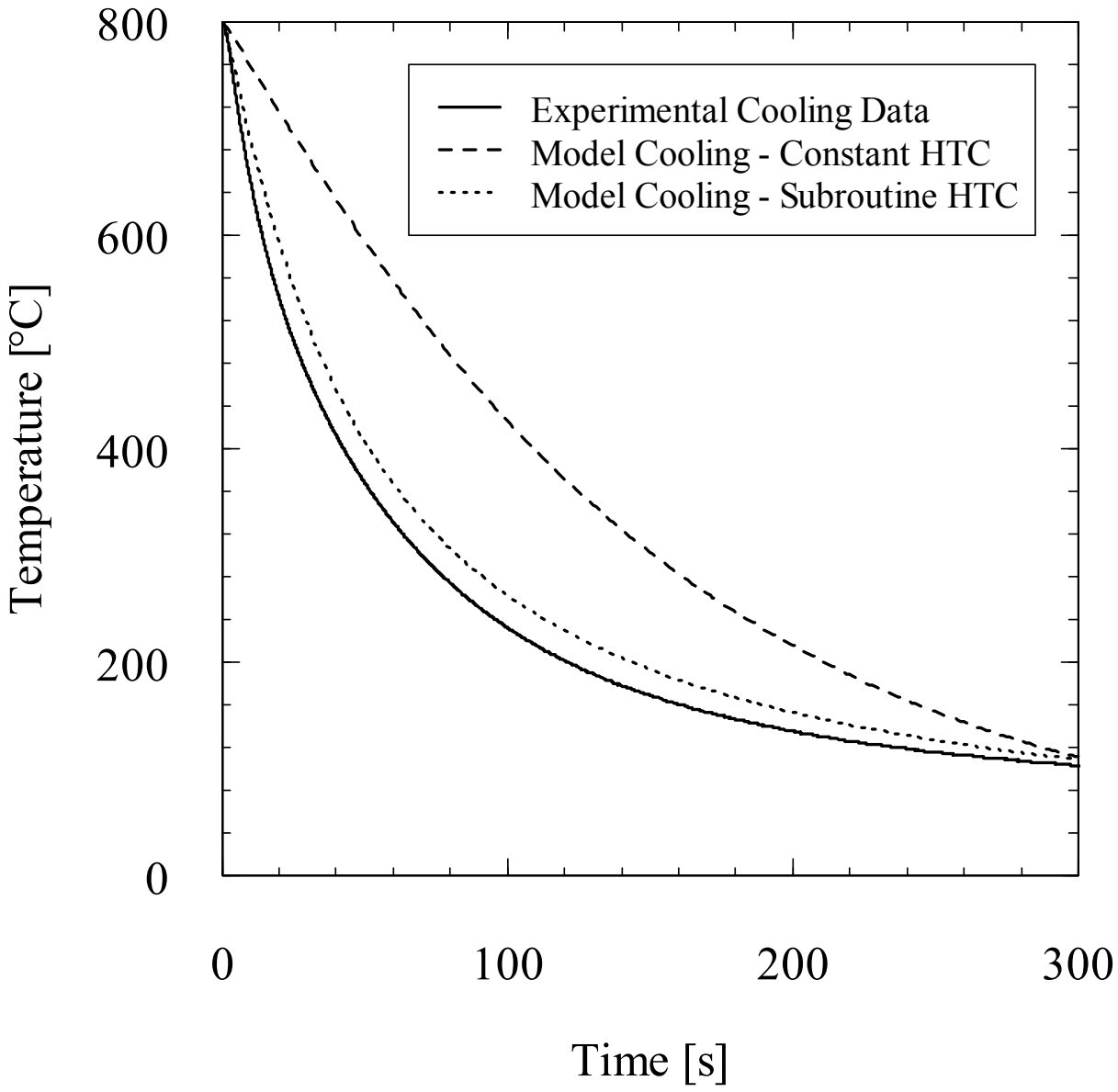

Figure 16: Comparison between experimental cooling from 800°C with Gleeble model using constant value and subroutine HTCs

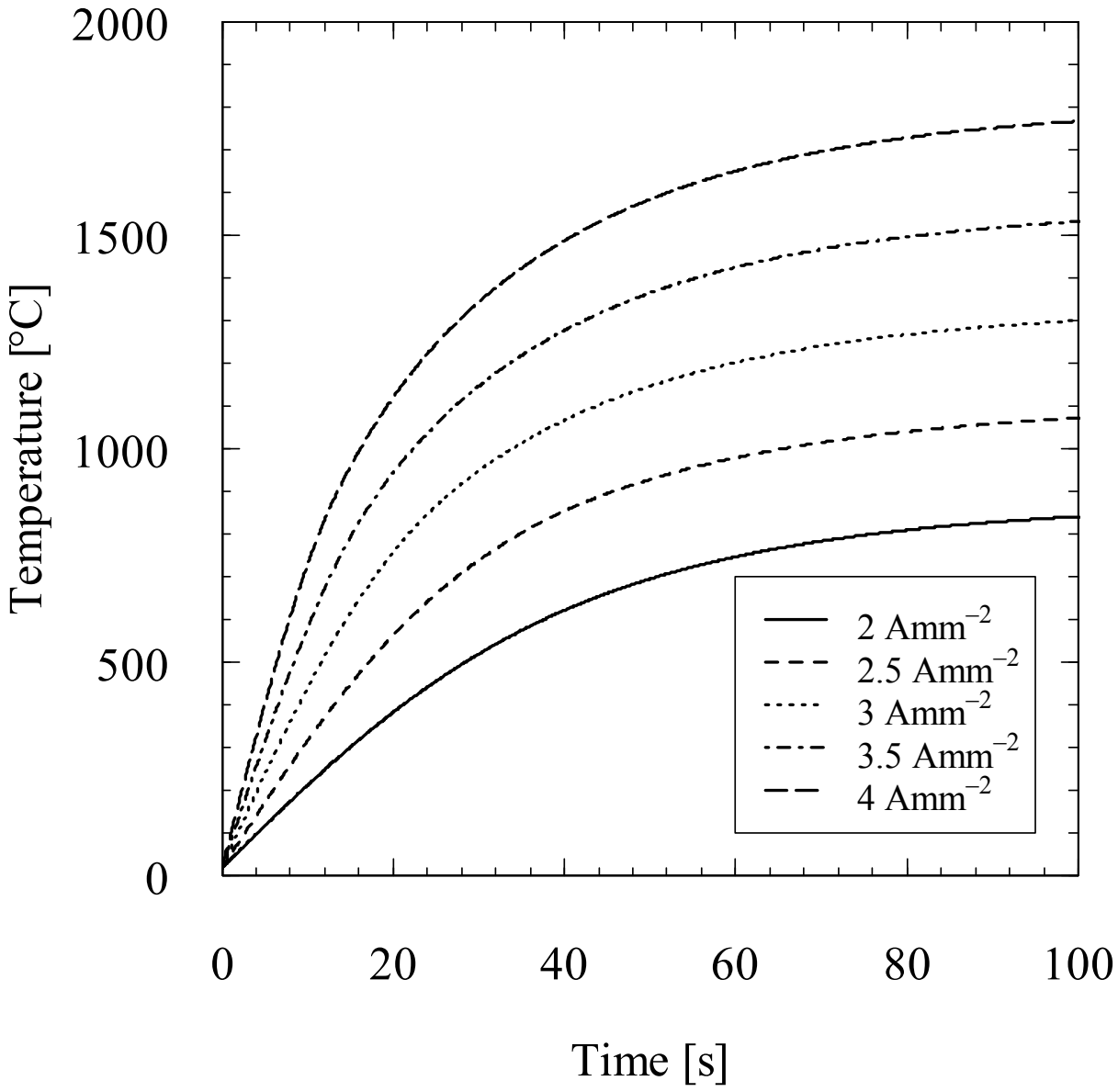

Figure 17: Gleeble model mid-axial point temperature profiles for different applied current fluxes

4.3 Heat generation in the specimen due to resistance heating

At present only a constant value of applied current flux can be used in a DEFORM model. Model results for temperature-time profiles from the mid-axial point (the control thermocouple position in the experiment) for different values of applied current flux on the platens are shown in Figure 17. Heating rates to the target temperatures have been extracted from these results and a value of current flux which gives approximately linear heating to the target temperature has been determined

in order to recreate the conditions of heating used during the testing. This is shown in Figure 18; linear fits to the heating rates against applied current fluxes are shown for target temperatures of 800 and 1100°C. The linear fits suggest current fluxes of 2.38 and 2.84 Amm^{-2} for heating rates of 20°Cs^{-1} to 800 and 1100°C respectively.

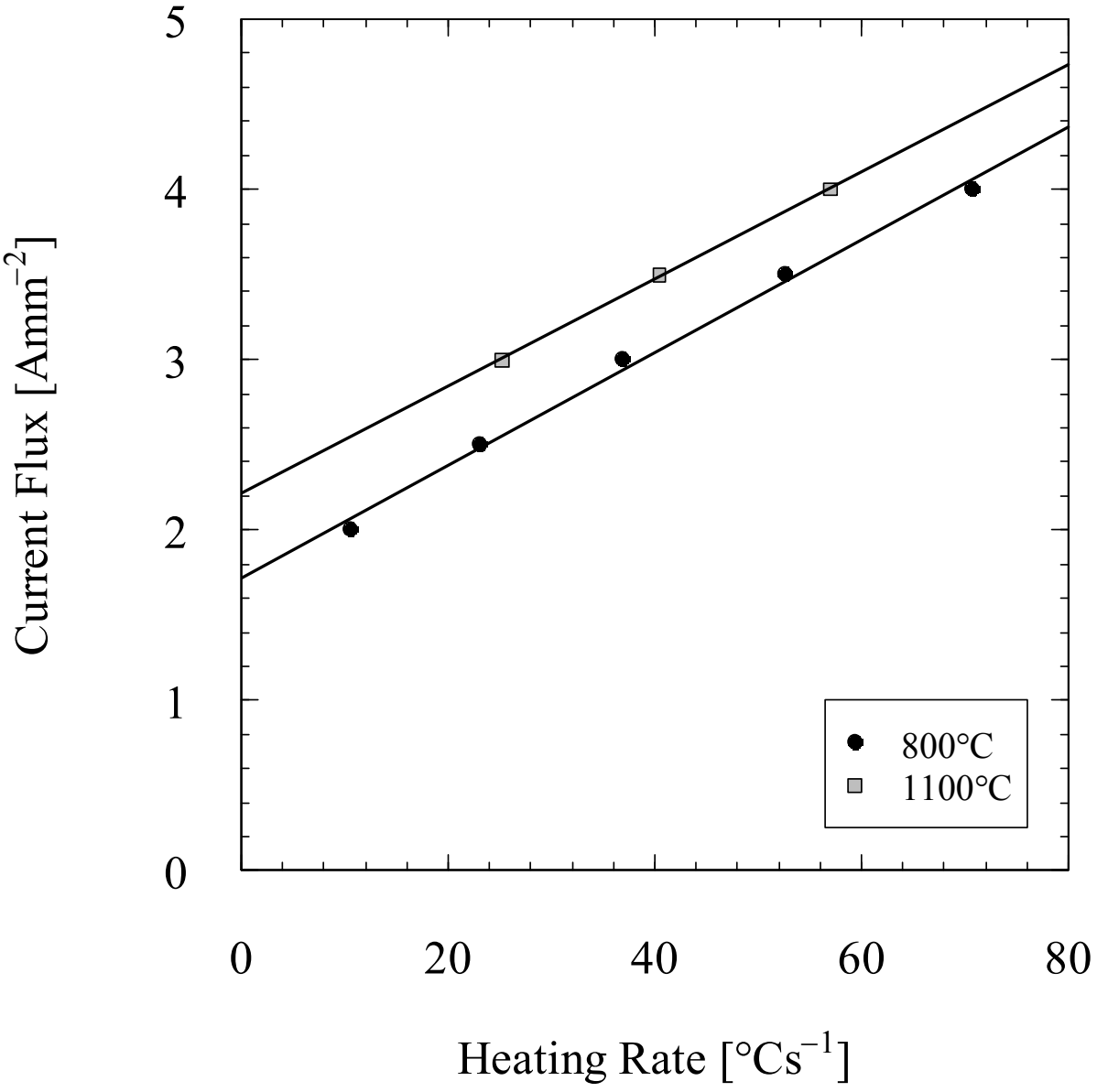

Figure 18: Current flux required for heating rate to 800 and 1100°C from Figure 17

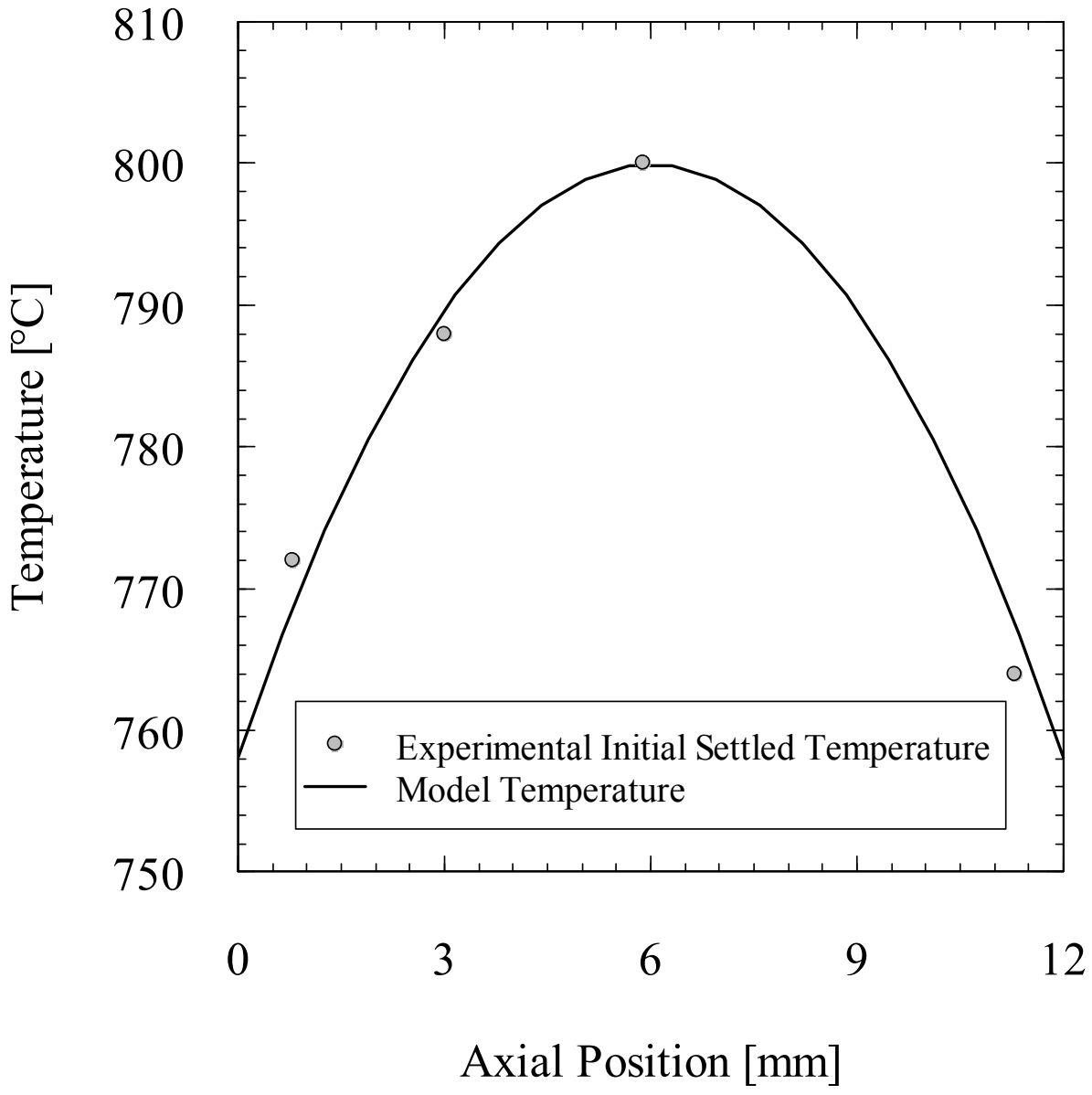

Figure 19: Modelled axial temperature distribution in Gleeble specimen at 800°C compared with experimental data

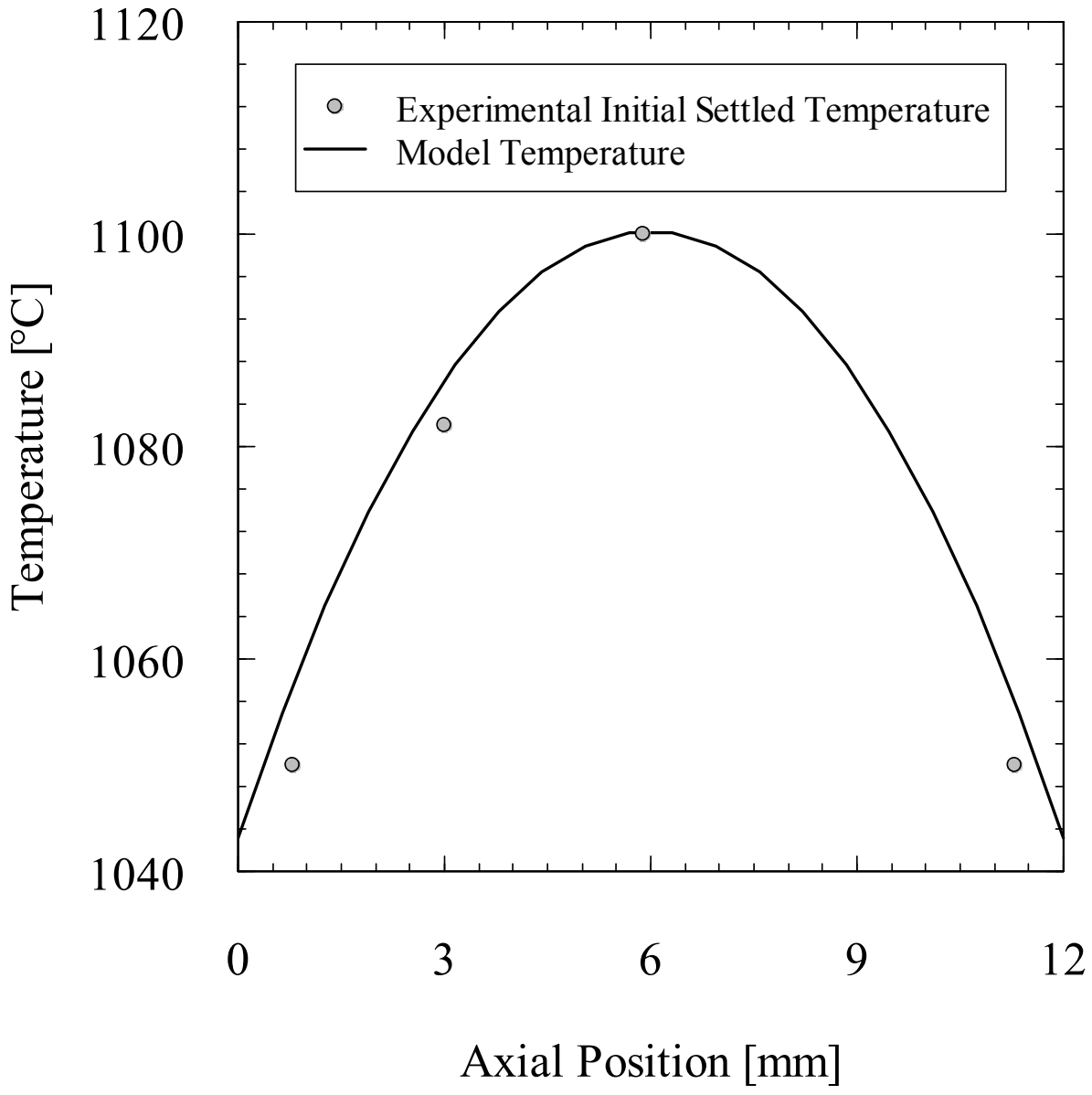

Figure 20: Modelled axial temperature distribution in Gleeble specimen at 1100°C compared with experimental data

Table 2: Gleeble model heating details

Current Flux	2.84	2.38	$As^{-1}mm^{-2}$
Temp.	1100	800	°C
Time to Temp.	53.4	40.1	s
Heating Rate	20.60	19.95	$°Cs^{-1}$

The results of the heating models(incorporating both heat generation due to joule heating and heat loss from the free and contacting surfaces) using the subroutine HTCs are presented and compared with the experimental temperature profiles [21] in Figure 19 and Figure 20, good agreement is achieved. Linear heating rates to 800°C and 1100°C are compared for the calculated current fluxes in Table 2 and show that the achieved values in the model are very close to the target value of 20°Cs^{-1}. These results show the applicability of the present Gleeble heating model (via the subroutine) throughout the high temperature testing range.

4.4 Stress/strain measurement in Gleeble testing

In Gleeble compression testing, the dilation at the largest part of the specimen is measured using a C-gauge and the true strain is determined using:

$$\varepsilon = 2\ln\left(\frac{D_0 + \Delta D}{D_0}\right) \qquad 24$$

The stress is calculated from the force measurements as follows:

$$\sigma = \frac{F}{\frac{\pi(D_0 + \Delta D)^2}{4}} \qquad 25$$

In the modelling work, the radial displacement of the mid-axial surface point is taken from the model output and Equation 24 is used to convert this to strain in a similar manner.

The strain measurement in Gleeble testing is clearly a more direct measurement than that employed for isothermal compression testing where the crosshead displacement is usually used and converted

to true strain, with some correction normally being applied in the latter case to account for test rig compliance [16].

4.5 Compression

As for the isothermal compression testing the velocity of the top platen/die is again defined as a function of height in the analysis to give constant macroscopic true strain rate as detailed in Equation 1.

The non-uniform deformation present in the sample is highlighted by the barrelled shape of the specimen and by the non-uniform strain contours presented in Figure 21. It can be seen that local strain values at a macroscopic axial true strain of 0.5 are in excess of 1, showing that the deformation in the centre of the specimen is far higher than the nominal conditions for the specimen when tested using the Gleeble method.

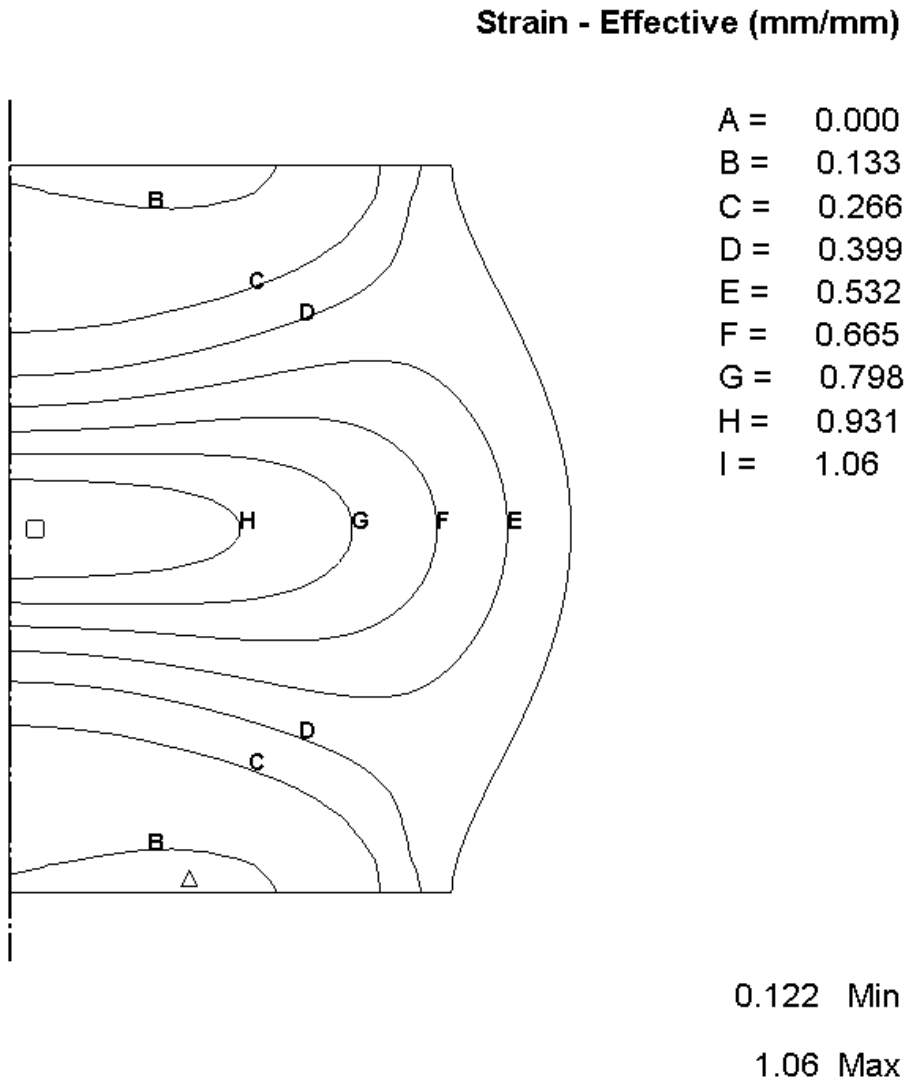

Figure 21: Gleeble model showing strain contours at a nominal axial true strain of 0.5 (T=1100°C, $\dot{\varepsilon}$=1s^{-1}, m=0, η=0)

The local radial strain data from the model are shown in Figure 22 and are compared to the calculated axial strain values. It can be seen that the radial strain values are higher than the axial strains and that they also vary non-linearly unlike the axial strain profile which is linear. When viewed as strain rate in Figure 23, it can be seen that the initial strain rate value in this case (T=1100°C, $\dot{\varepsilon}$=1s^{-1}, m=0) is over 80% higher than the target value.

Axial strain rate profiles are shown at different strain levels along the centre of the specimen in Figure 24. This shows very high initial strain rates at the centre of the specimen due to the higher temperatures in this region which causes softening of the material. As the test proceeds, the strain rates gradually reduce in the centre of the specimen and increase at the specimen ends.

Figure 25 shows a comparison of the stress-strain curves derived from both the modelled axial strain data and the local dilation data at the axial centre of the specimen. This clearly shows that the local measurement of the strain gives a lower stress value for the material as the deformation is localised in the centre of the specimen due to the initial temperature profile. The errors when compared to the reference stress value from the material model for these conditions are shown in Figure 26. Large errors are seen at the beginning of the test due to the increased strain rate at the centre of the specimen where the most deformation is occurring. For an 80% increase in strain rate Equation 3 gives a 10% increase in flow stress of the material. This 80% strain rate increase is however based on the average measurement of strain rate across the axial central plane of the specimen and strain rates in the core of the specimen are higher. This increases the material strength and results in the initial errors of 15% seen in Figure 26.

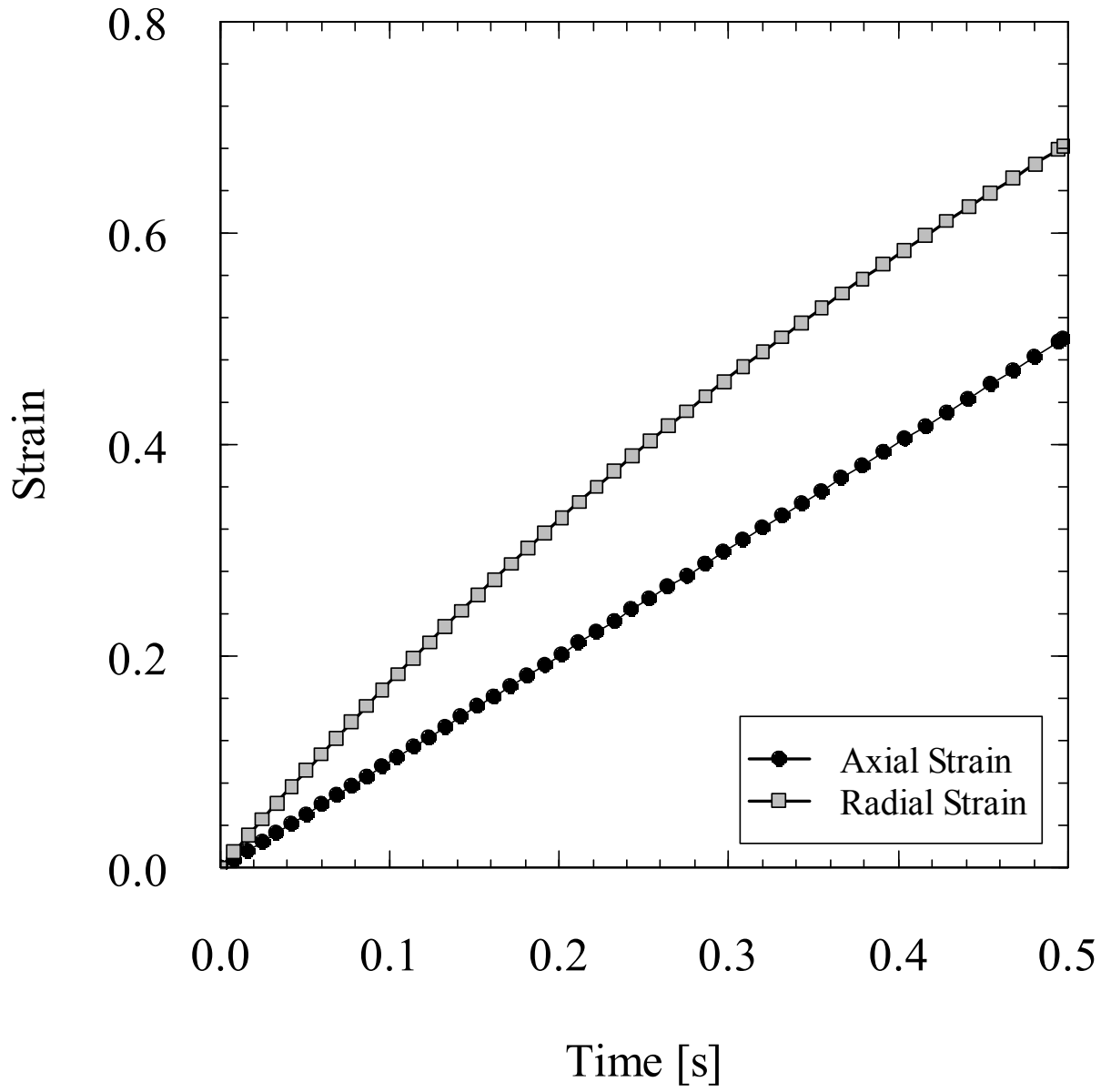

Figure 22: Comparison of axial and radial strain interpretation from Gleeble compression model (T=1100°C, $\dot{\varepsilon}$ =1s^{-1}, m=0, η=0.9)

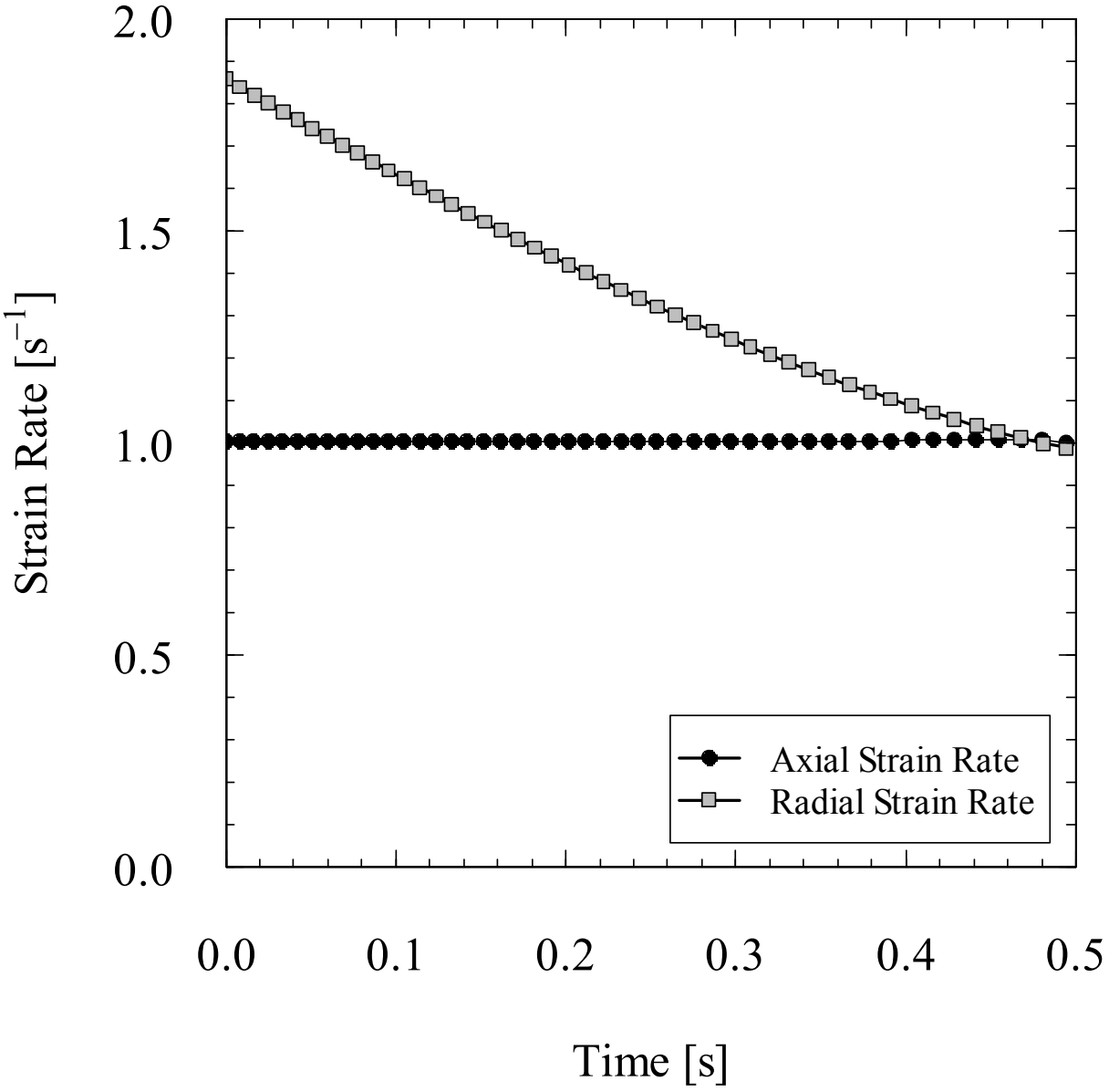

Figure 23: Comparison of radial and axial strain rate interpretation from Gleeble compression model (T=1100°C, $\dot{\varepsilon}$=1s^{-1}, m=0, η=0.9)

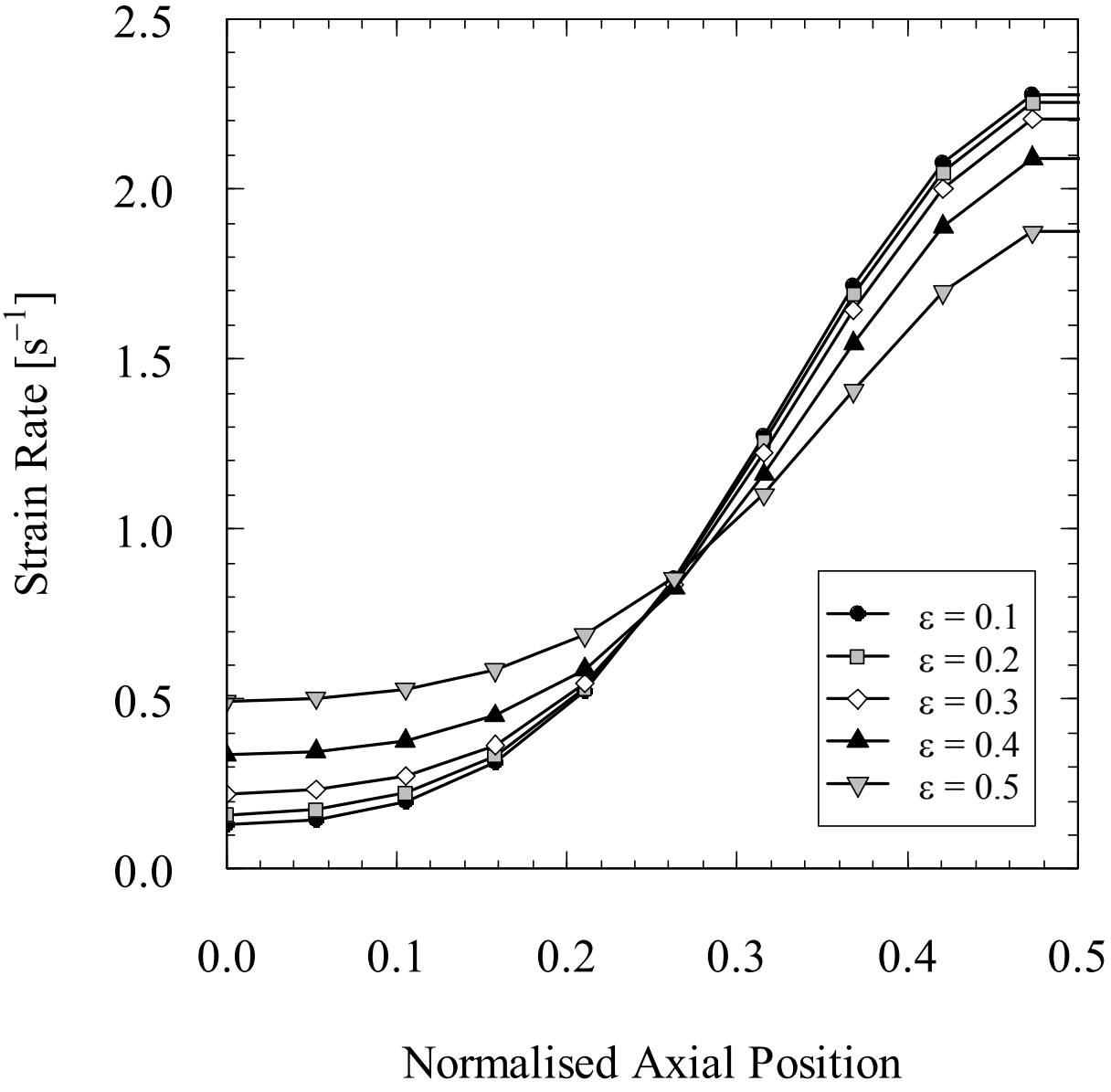

Figure 24: Evolution of strain rate with increasing strain within Gleeble specimen model (T=1100°C, $\dot{\varepsilon}$=1s^{-1}, m=0, η=0.9)

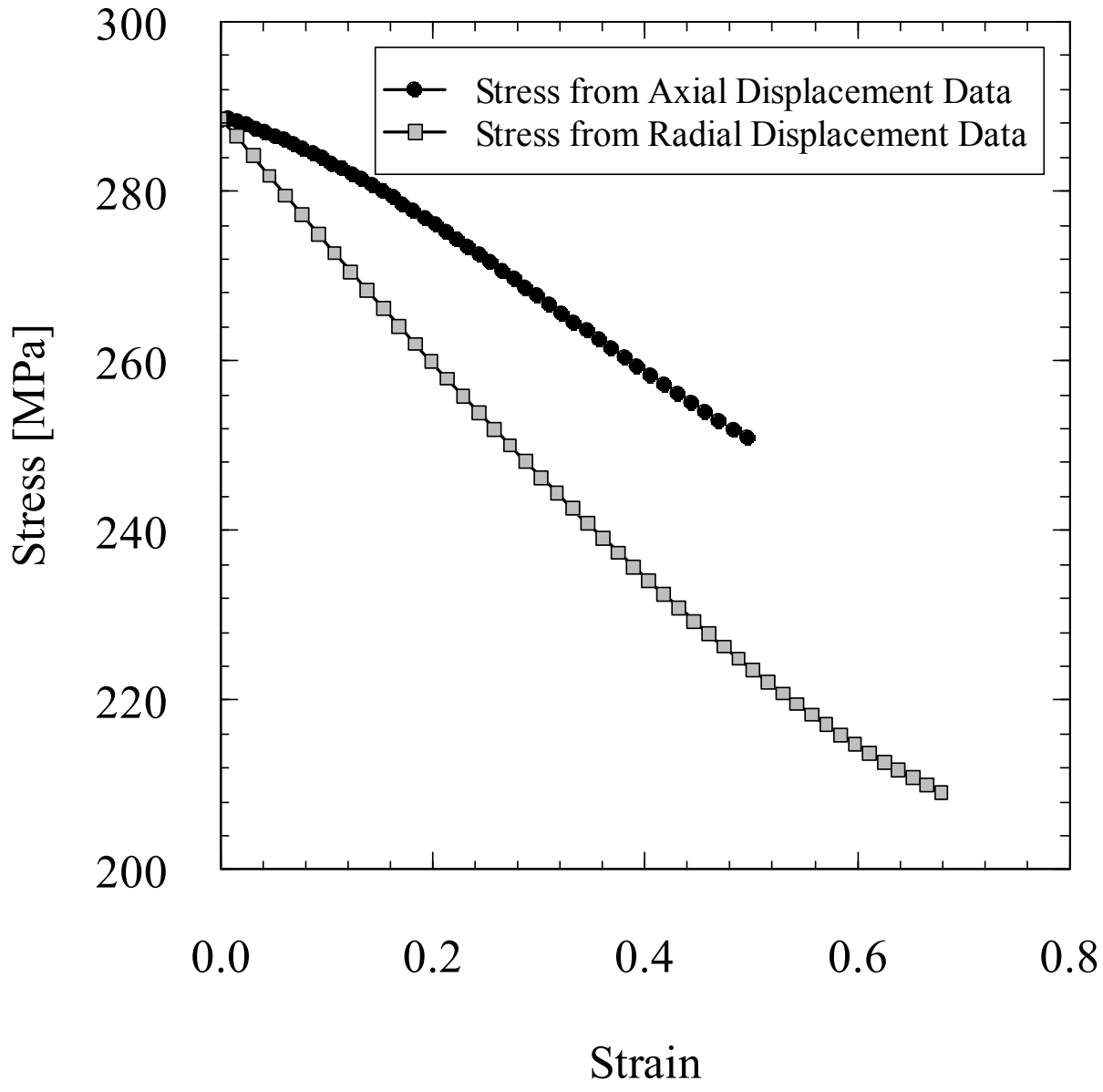

Figure 25: Comparison of stress-strain curves derived from axial and radial displacement measurements (T=1100°C, $\dot{\varepsilon}$ =1s^{-1}, m=0, η=0.9)

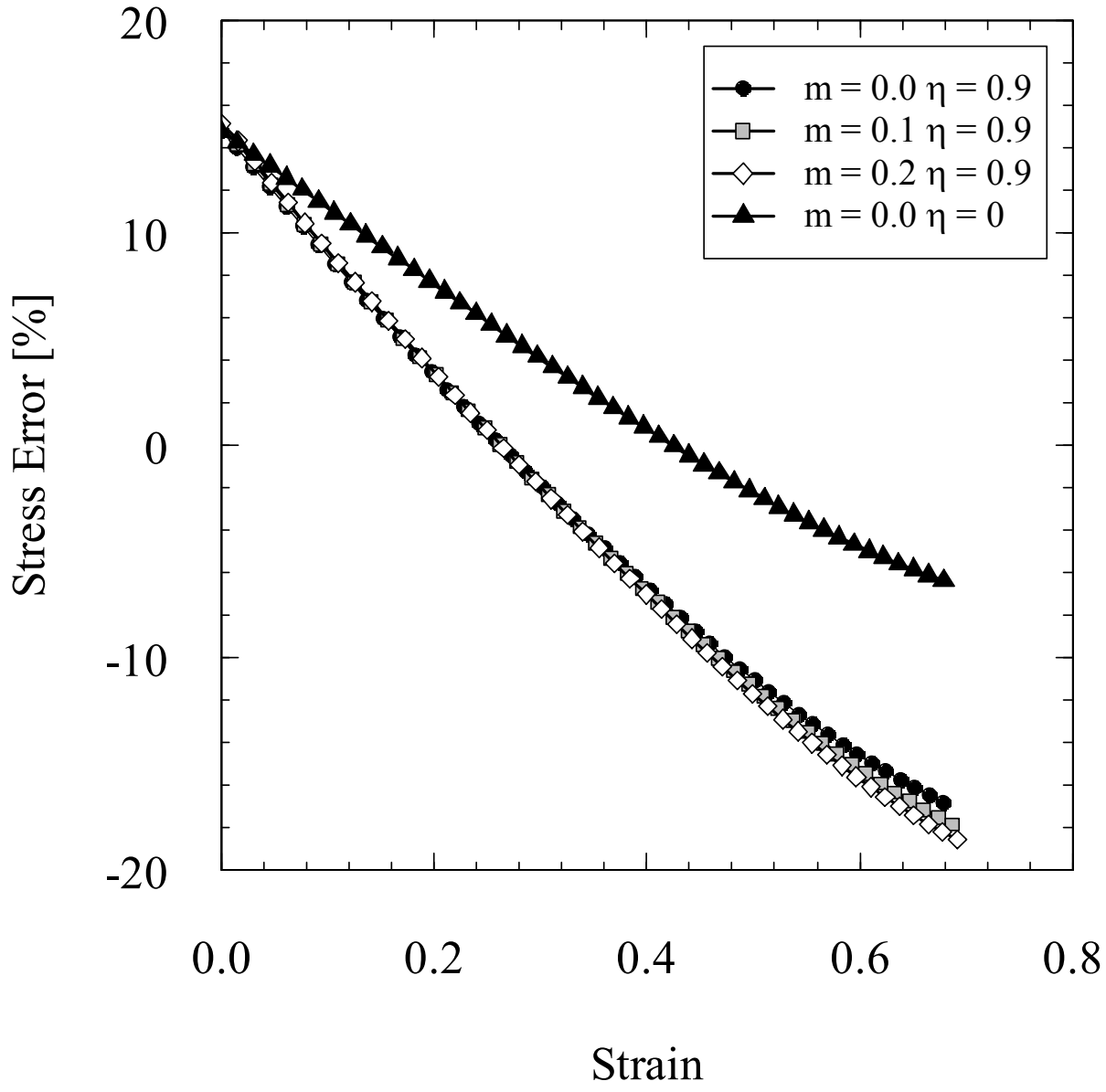

Figure 26: Comparison of relative stress errors from Gleeble compression models (*T*=1100°C, $\dot{\varepsilon}$=1s^{-1})

Figure 26 also shows how the errors are affected by the interface coefficient of friction. This effect (of *m*) is seen to be insignificant. Also shown is the error including the heating effects due to plastic deformation during the test; this adds an extra 10% to the error seen in the Gleeble test by increasing the material softening. This compares well with the additional error added under the

same conditions (T=1100°C, $\dot{\varepsilon}$=1s^{-1}) in the isothermal compression testing model when the heating due to plastic deformation was considered (Figure 10).

5 Comparison of Isothermal and Gleeble Test Models

A comparison of the results from the models for both the isothermal and Gleeble tests is made using the same nominal testing conditions (T=1100°C, $\dot{\varepsilon}$=1s^{-1}, m=0.2, η=0.9). Stress-strain curves derived by the methods appropriate for each model are presented in Figure 27. The effect of flow softening due to heating from plastic deformation can clearly be seen in both stress-strain curves as the perceived strength of the material reduces.

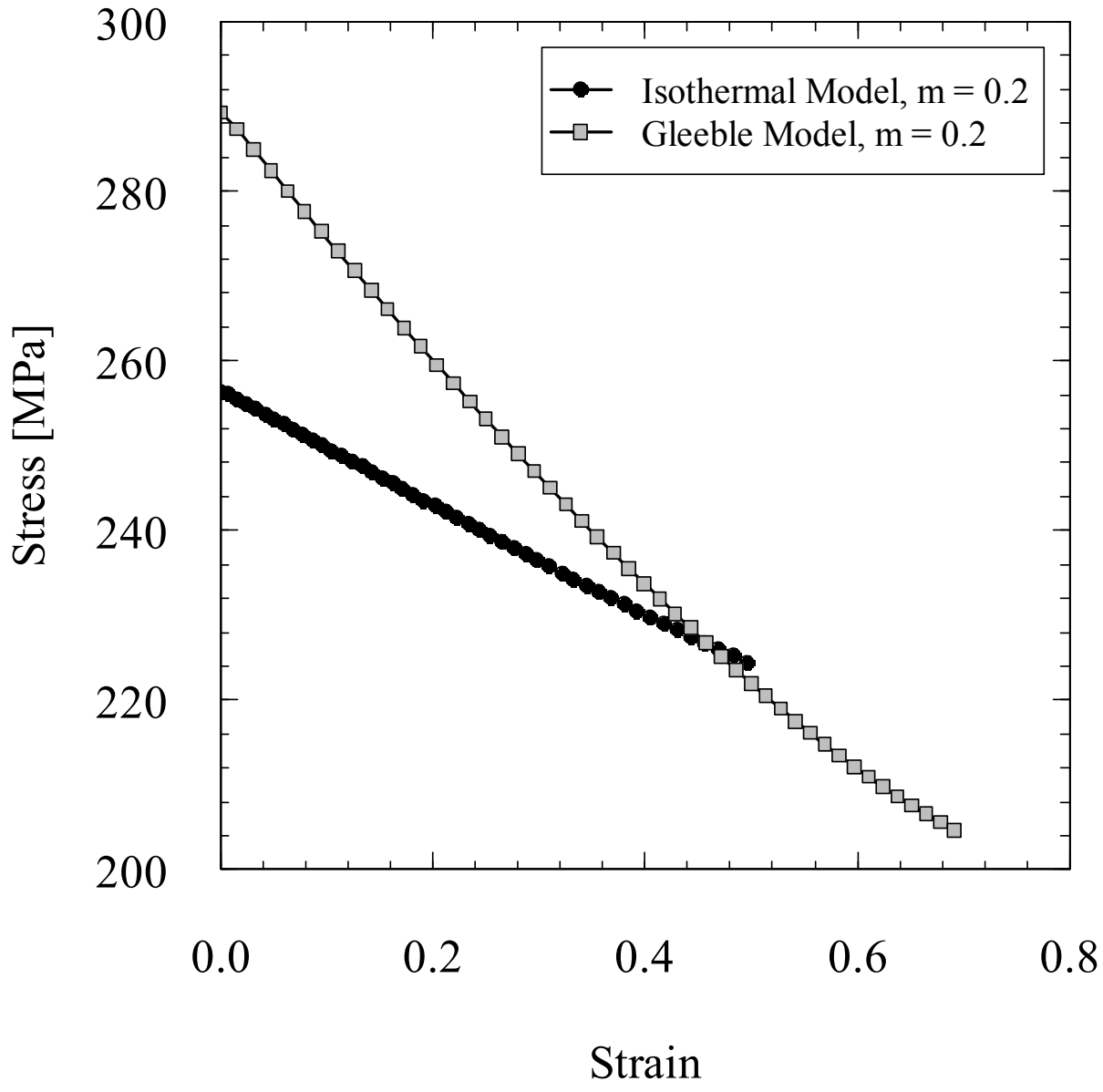

Figure 27: Comparison of stress-strain curves generated from isothermal and Gleeble models (T=1100°C, $\dot{\varepsilon}$=1s^{-1}, m=0.2, η=0.9)

Relative stress errors from both models under the same nominal conditions are presented in Figure 28. It can be seen that the errors from the Gleeble model are far higher than those from the Isothermal model with initial values starting at significant positive values. These initial errors then drop to negative values due to heating from plastic deformation as the sample is compressed.

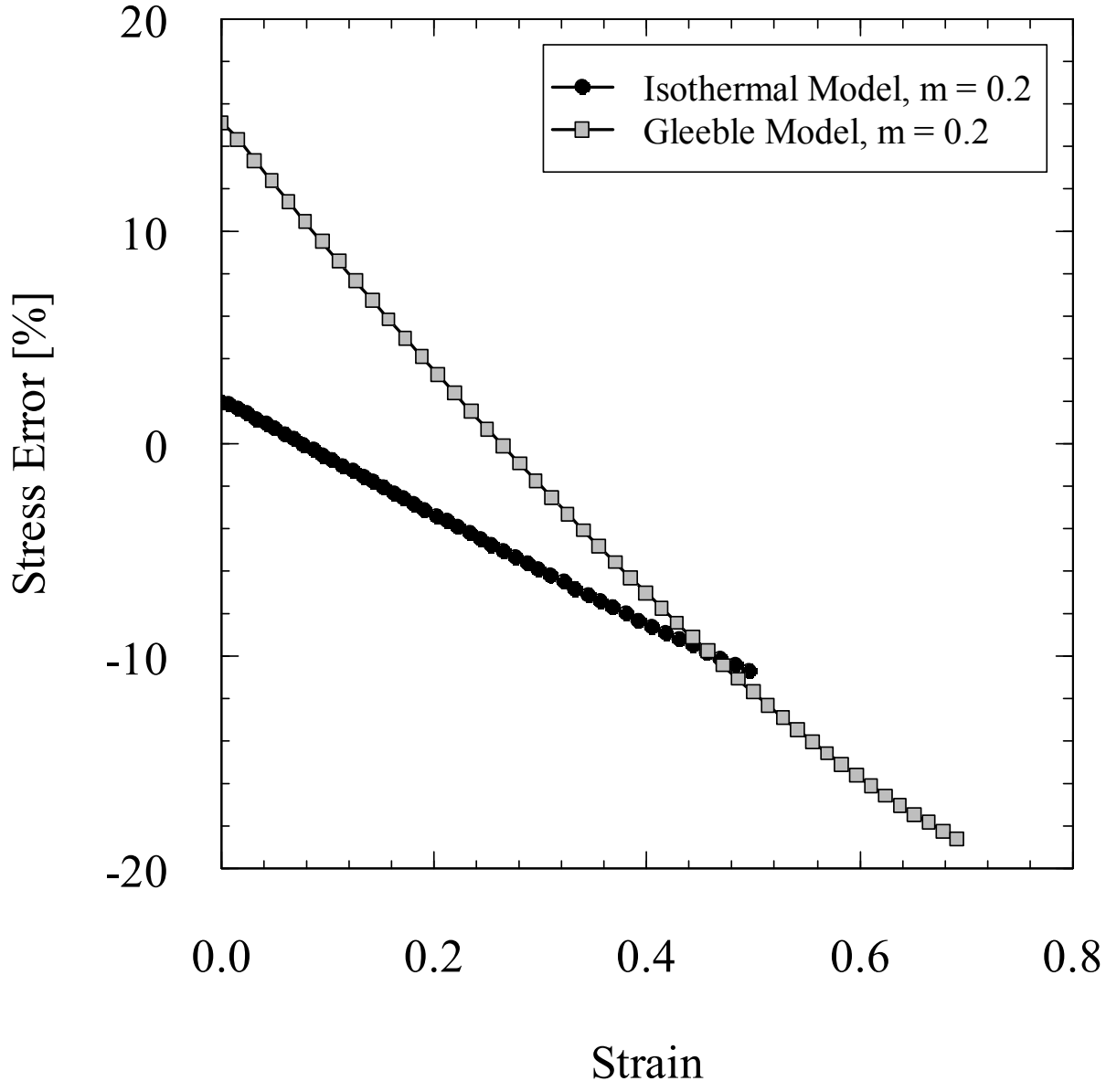

Figure 28: Comparison of relative stress error from isothermal and Gleeble models (T=1100°C, $\dot{\varepsilon}$=1s^{-1}, m=0.2, η=0.9)

The high local strain rates in the Gleeble model are highlighted in Figure 29 where the effective strain rates are compared along the centreline of the specimen between both the isothermal and Gleeble models early in the test (strain = 0.1) and the point at which the test was stopped (strain = 0.5). It can be seen that although the values change as the sample is compressed, the strain rate in

the Gleeble model remains higher in the centre throughout the test and local values in the centre of the specimen are nearly double those from the isothermal model.

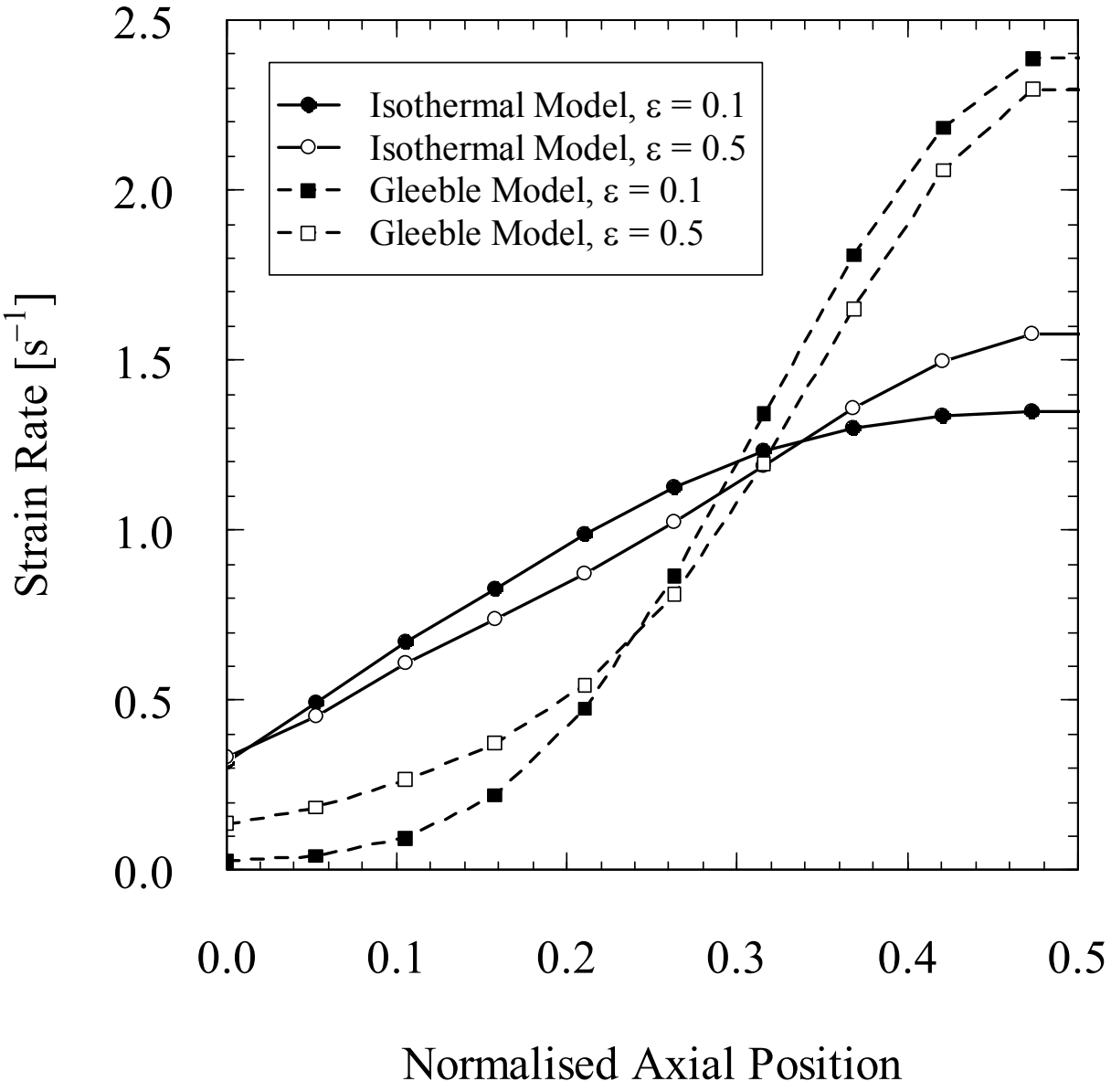

Figure 29: Comparison of strain rates along the centreline of both the isothermal and Gleeble models at two strain levels (T=1100°C, $\dot{\varepsilon}$=1s^{-1}, m=0.2, η=0.9)

6 Conclusions

Modelling of both the isothermal compression test and the compression test using the Gleeble thermomechanical simulator has shown that errors are present in both tests due to the non-uniform deformation (caused by friction at the interface) and temperature fields and the heating due to plastic deformation. Errors are significantly higher for the Gleeble model when compared to the isothermal model due to the initial temperature profile in the specimen which results in local deformations at the axial centre for the specimen, this causes higher local strain rates and higher associated strength (compared to nominal strain rate conditions).

The Gleeble compression testing method has advantages for generating flow stress data for some finite element process modelling due to the rapid heating which can be applied to the specimens which avoids unwanted microstructural changes in the material. However this work has highlighted the importance of applying some correction or care when assigning strain rates and temperature values to Gleeble flow stress. During the initial part of the test, positive errors are predicted due to higher than nominal strain rates; the errors drop off due to reducing strain rates and softening due to heating from plastic deformation.

Interface resistance between the specimen and platens has not been taken in to account, however this could be an important effect and differences in this value between the contacting surfaces could result in skewing of the temperature profile and non-axisymmetric deformations.

Acknowledgements

The authors would like to thank Rolls-Royce plc, Aerospace Group. The views expressed in this paper are those of the authors and not necessarily those of Rolls-Royce plc, Aerospace Group. The authors would also like to thank The University of Birmingham for the experimental temperature

data regarding the Gleeble thermomechanical simulator and Swansea University for the material compression data used in this work. This work has been carried out under the PROMOTE project funded by The Technology Strategy Board. The Technology Strategy Board is a business-led executive non-departmental public body, established by the government. Its mission is to promote and support research into, and development and exploitation of, technology and innovation for the benefit of UK business, in order to increase economic growth and improve the quality of life. It is sponsored by the Department for Innovation, Universities and Skills (DIUS). Please visit www.innovateuk.org for further information.

References

1. Onawola, O.O. and M.B. Adeyemi, *Warm compression and extrusion tests of aluminium.* Journal of Materials Processing Technology, 2003. **136**(1-3): p. 7-11.
2. Chen, Z.H., M.Y. Zhan, and W.J. Xia, *Deformation and fracture behaviour of porous FVS0812 aluminium alloy prepared by spray deposition.* Materials Science and Technology, 2004. **20**(12): p. 1621-1626.
3. Hwu, Y.-J., C.-T. Hsu, and F. Wang, *Measurement of friction and the flow stress of steels at room and elevated temperatures by ring-compression tests.* Journal of Materials Processing Technology, 1993. **37**(1-4): p. 319-335.
4. Kang, F.-w., et al., *Hot deformation of spray formed nickel-base superalloy using processing maps.* Transactions of Nonferrous Metals Society of China, 2008. **18**(3): p. 531-535.
5. Nawrocki, P.A., M.B. Dusseault, and R.K. Bratli, *Use of uniaxial compression test results in stress modelling around openings in nonlinear geomaterials.* Journal of Petroleum Science and Engineering, 1998. **21**(1-2): p. 79-94.
6. Evans, R.W. and P.J. Scharning, *Axisymmetric compression test and hot working properties of alloys.* Materials Science and Technology, 2001. **17**: p. 995-1004.
7. Evans, R.W. and P.J. Scharning, *Strain inhomegeneity in hot axisymmetric compression test.* Materials Science and Technology, 2002. **18**: p. 1389-1398.
8. Brown, S.G.R., J.D. James, and J.A. Spittle, *3D numerical model of the temperature-time characteristics of specimens tested on a Gleeble thermomechanical simulator.* Modelling and Simulation in Materials Science and Engineering, 1997. **5**(6): p. 539-548.
9. Chen, D.-C., *Rigid-plastic finite element simulation of deformation mechanisms during rolling of complex sheets containing an inclusion.* Key Engineering Materials, 2006. **306-308 I**: p. 483-488.
10. Liang, S.J., Z.Y. Liu, and E.D. Wang, *Simulation of extrusion process of AZ31 magnesium alloy.* Materials Science and Engineering A, 2009. **499**(1-2): p. 221-224.
11. O'Connell, M., et al., *Flashless closed-die upset forging-load estimation for optimal cold header selection.* Journal of Materials Processing Technology, 1996. **59**(1-2): p. 81-94.
12. Bennett, C.J., T.H. Hyde, and E.J. Williams, *Modelling and simulation of the inertia friction welding of shafts.* Proceedings of the Institution of Mechanical Engineers, Part L: Journal of Materials: Design and Applications, 2007. **221**(4): p. 275-284.
13. Wang, L., et al., *Energy-input-based finite-element process modeling of inertia welding.* Metallurgical and Materials Transactions B: Process Metallurgy and Materials Processing Science, 2005. **36**(4): p. 513-523.
14. Incropera, F.P., et al., *Introduction to Heat Transfer*. 5th ed. 2007: John Wiley & Sons.
15. Kobayashi, S., S.I. Oh, and T. Altan, *Metal Forming and the Finite-Element Method*. 1989: Oxford University Press, USA.
16. Roebuck, B., et al., *Measuring Flow Stress in Hot Axisymmetric Compression Tests*, NPL
17. Wilthan, B., et al., *Thermophysical properties of the Ni-based alloy Nimonic 80A up to 2400 K, III.* Thermochimica Acta, 2007. **465**(1-2): p. 83-87.
18. Churchill, S.W. and H.H.S. Chu, *Correlating equations for laminar and turbulent free convection from a horizontal cylinder.* International Journal of Heat and Mass Transfer, 1975. **18**: p. 1049-1053.
19. Morgan, V.T., *The overall convective heat transfer from smooth circular cylinders.* Advances in heat transfer, 1975. **11**: p. A76-17076.
20. Doel, T., *Personal Communication on Cooling Profiles*, 2008

21. Doel, T., *Personal Communication on Gleeble Temperature Profiles.* 2008.